Supporting Information

Photo-Electroswitchable Arylaminoazobenzenes

Carl Jacky Saint-Louis,‡ David J. Warner,‡ Katie S. Keane, Melody D. Kelley, Connor M. Meyers, Silas C. Blackstock*

blackstock@ua.edu

Department of Chemistry & Biochemistry, The University of Alabama, Tuscaloosa, AL 35487-0336

Azobenzene, nanotechnology, photochemistry, molecular machine, switching, electrochemistry.

Table of Contents

1. ^{1}H NMR and ^{13}C NMR spectra

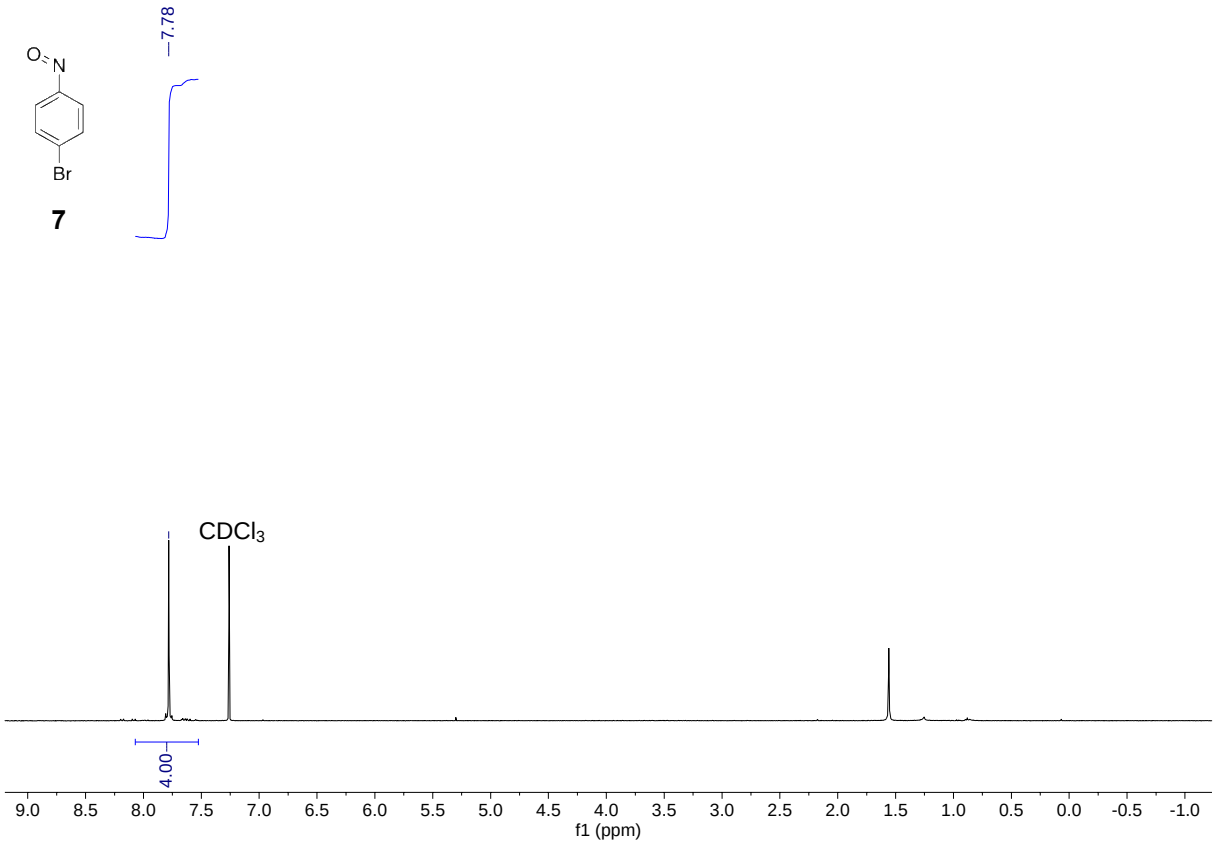

Figure S1. ^{1}H NMR spectrum (360 MHz) of **7** in $CDCl_3$

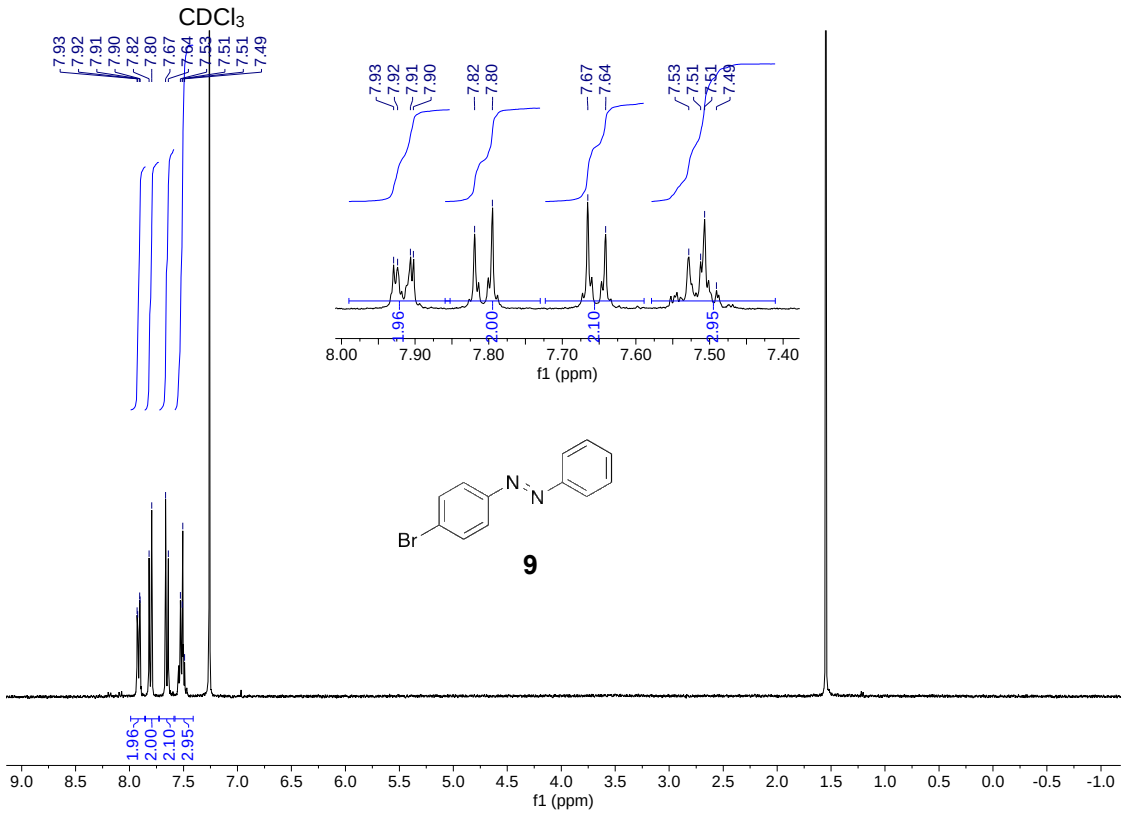

Figure S2. ^{1}H NMR spectrum (360 MHz) of **9** in $CDCl_3$

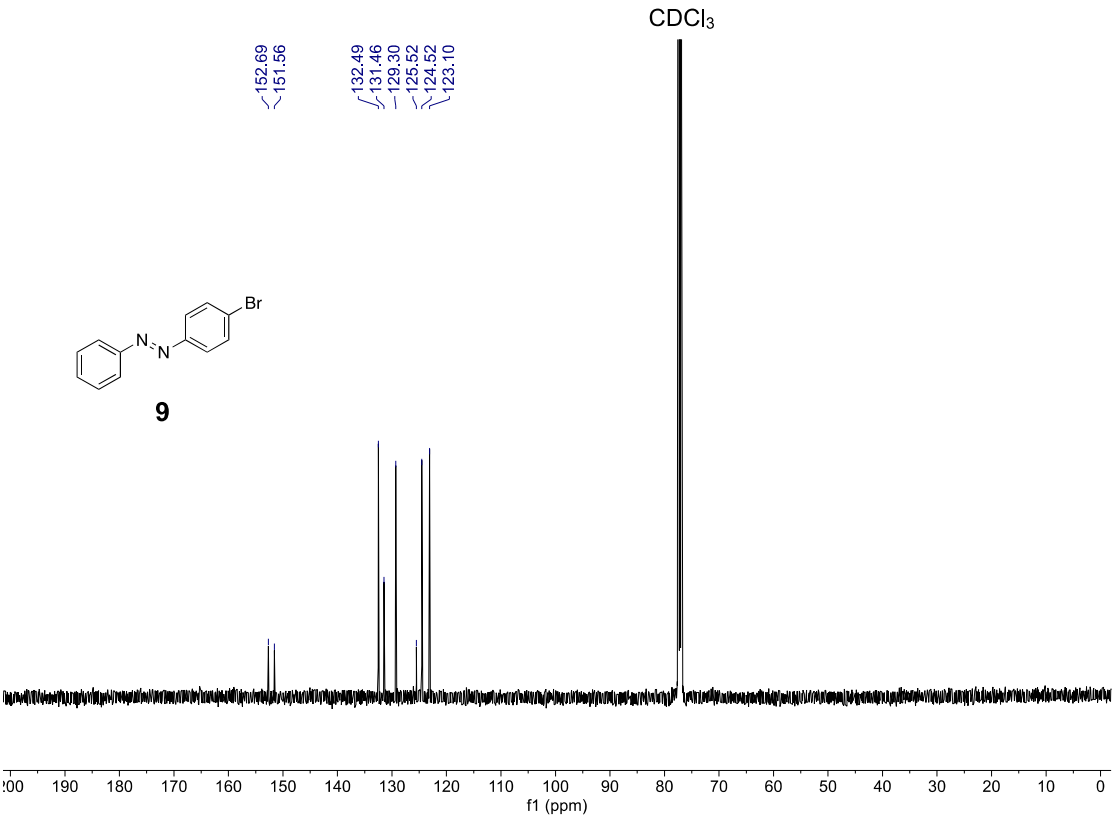

Figure S3. ^{13}C {^{1}H} NMR spectrum (125 MHz) of **9** in $CDCl_3$

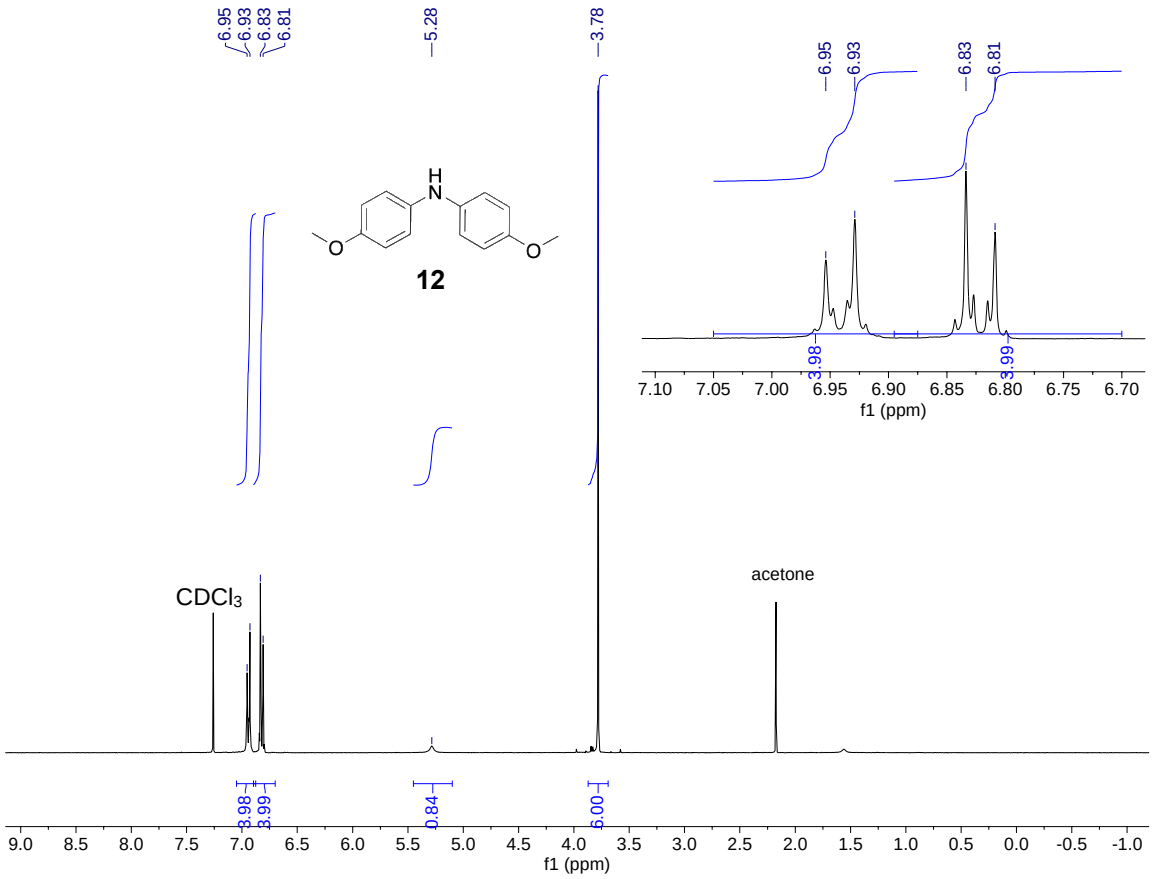

Figure S4. ^{1}H NMR spectrum (360 MHz) of **12** in $CDCl_3$

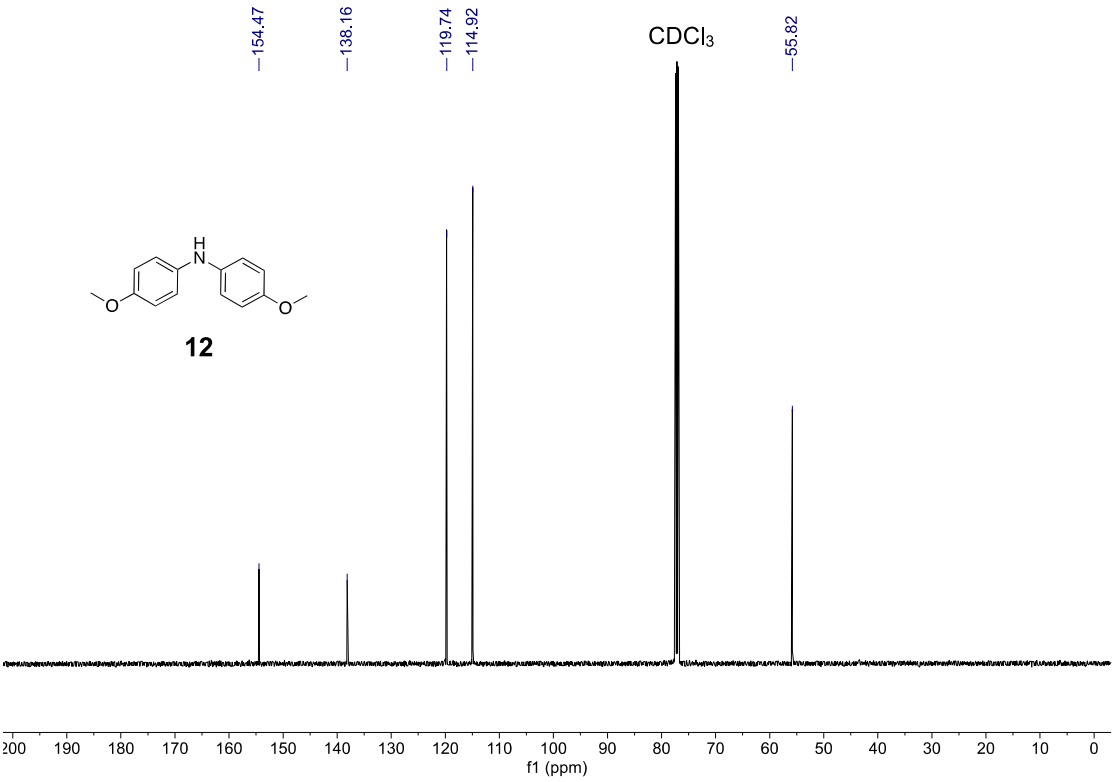

Figure S5. ^{13}C {^{1}H} NMR spectrum (125 MHz) of **12** in $CDCl_3$

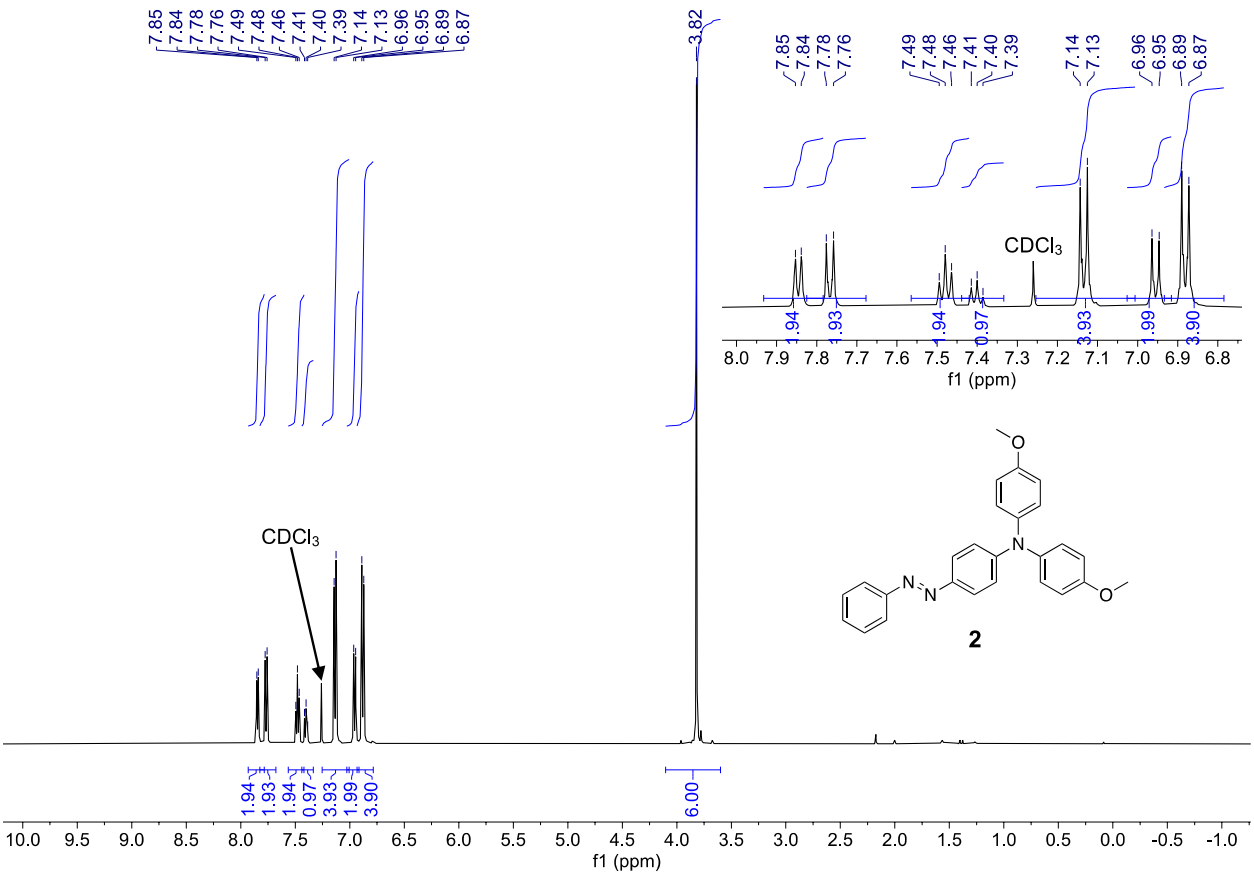

Figure S6. ^{1}H NMR spectrum (500 MHz) of **2** in $CDCl_3$

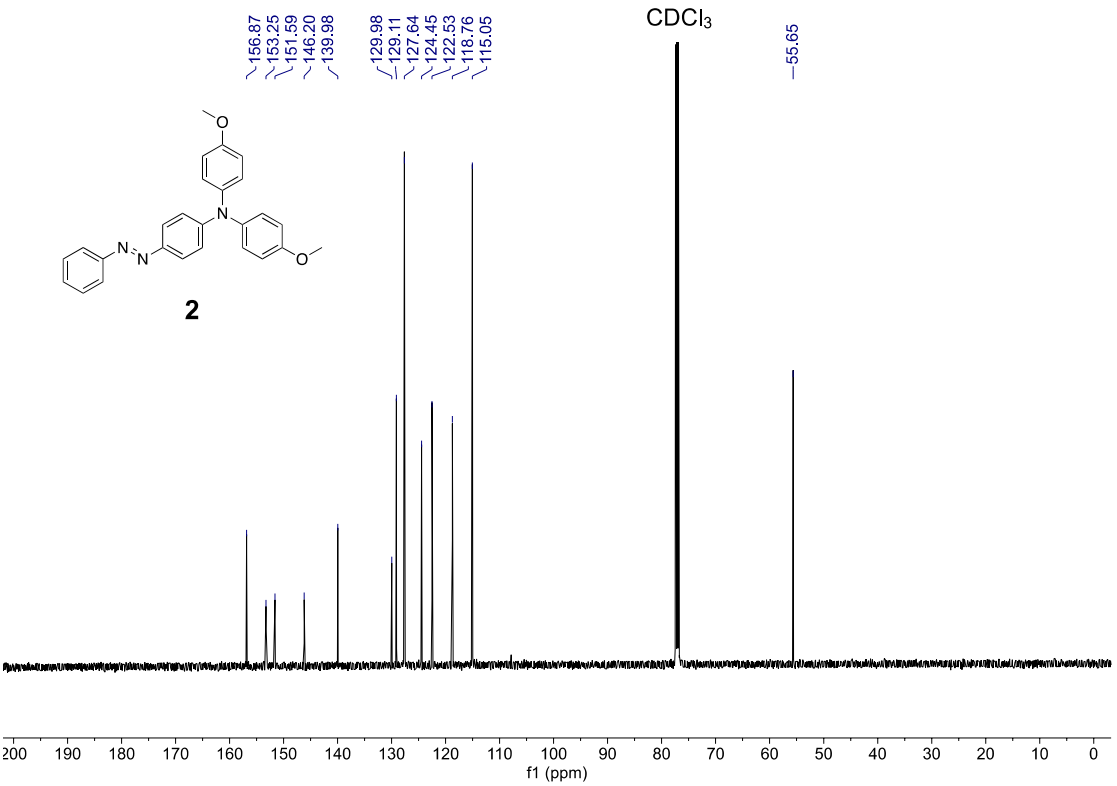

Figure S7. ^{13}C {^{1}H} NMR spectrum (125 MHz) of **2** in $CDCl_3$

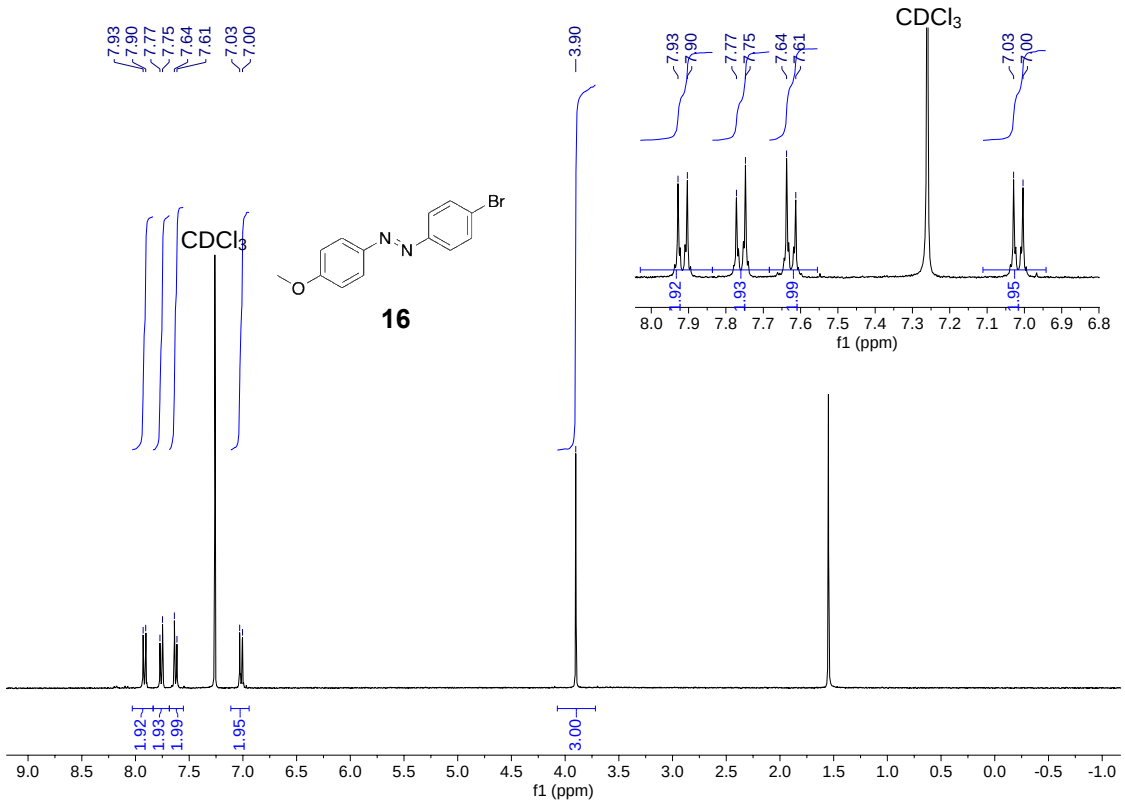

Figure S8. ^{1}H NMR spectrum (360 MHz) of **16** in $CDCl_3$

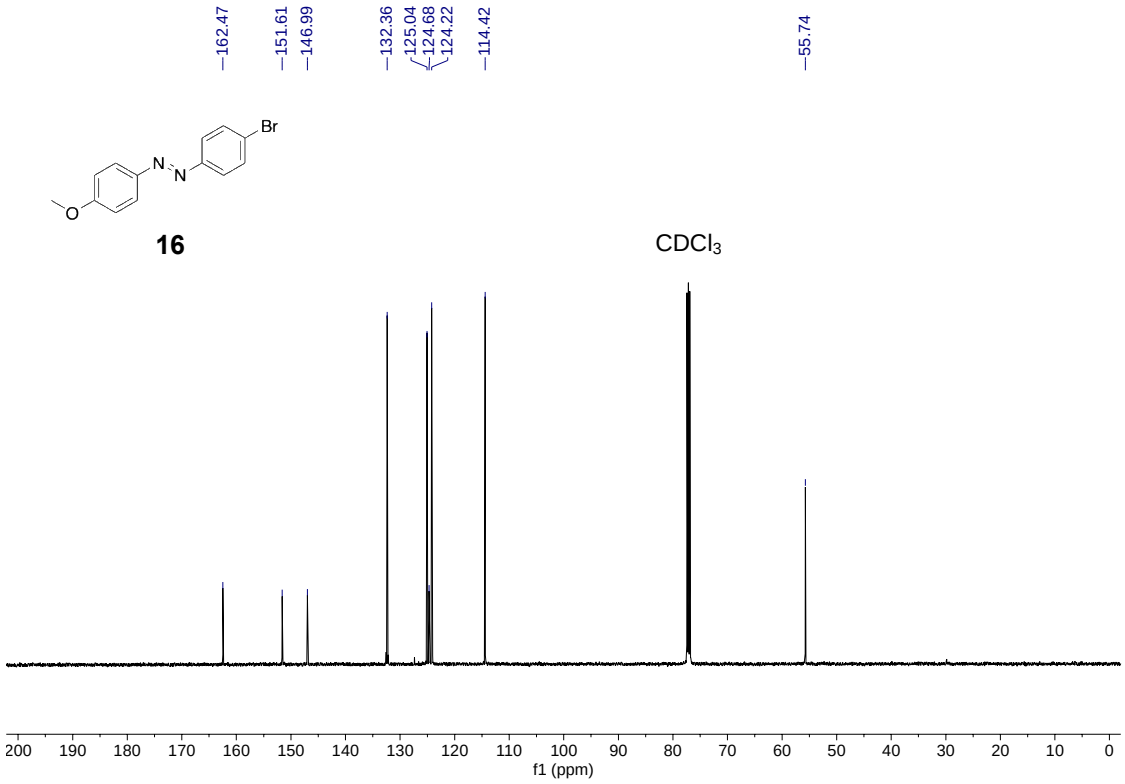

Figure S9. ^{13}C {^{1}H} NMR spectrum (125 MHz) of **16** in $CDCl_3$

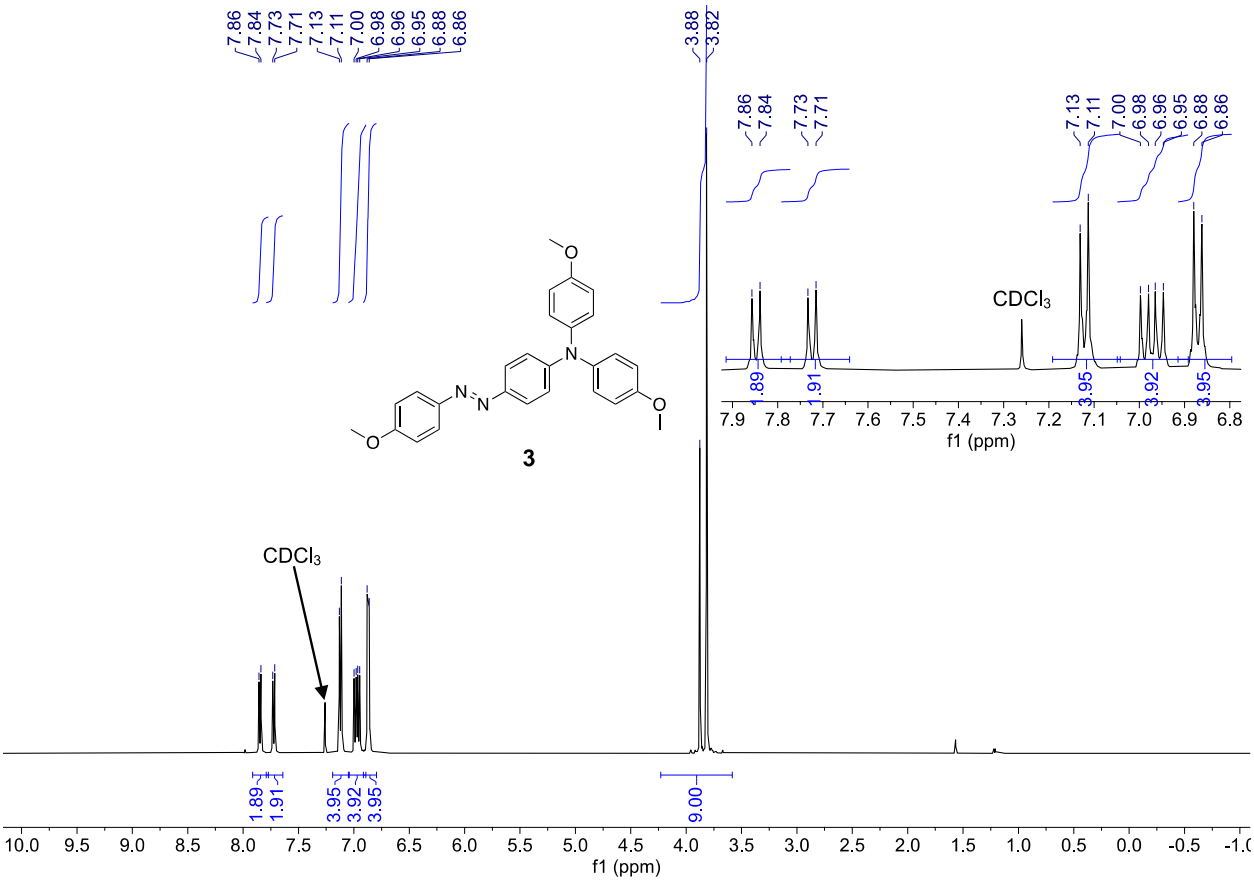

Figure S10. ^{1}H NMR spectrum (500 MHz) of **3** in $CDCl_3$

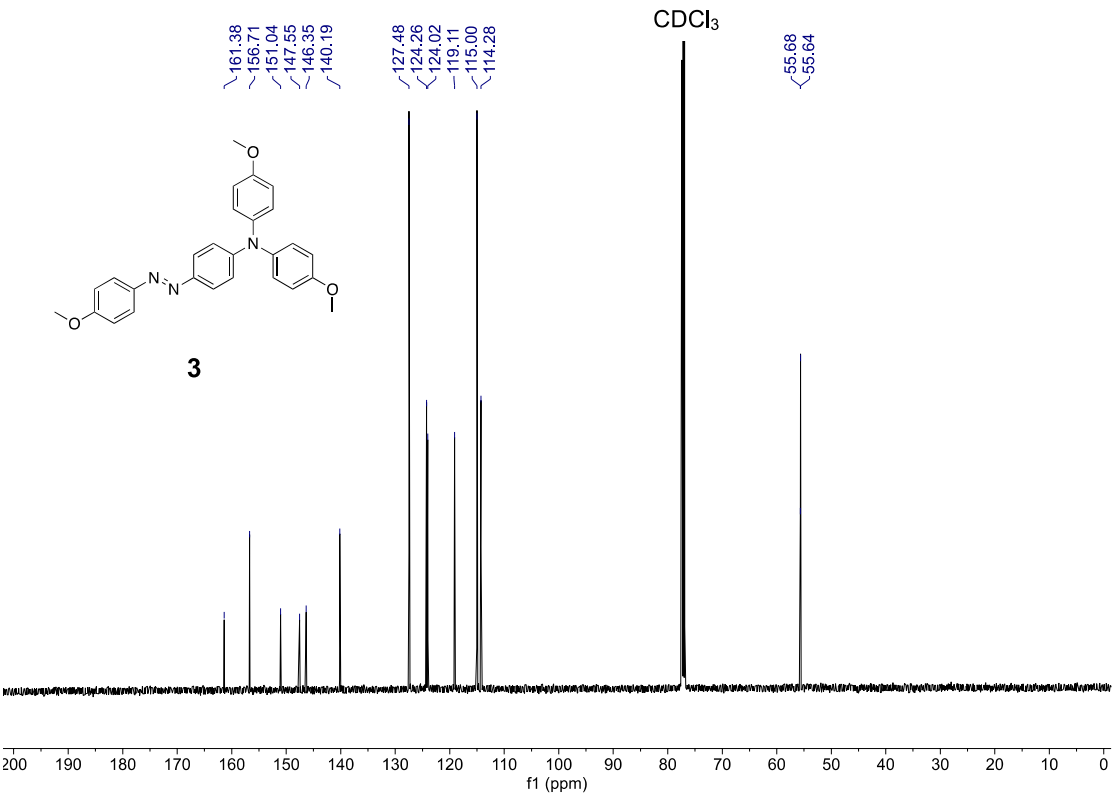

Figure S11. ^{13}C {^{1}H} NMR spectrum (125 MHz) of **3** in $CDCl_3$

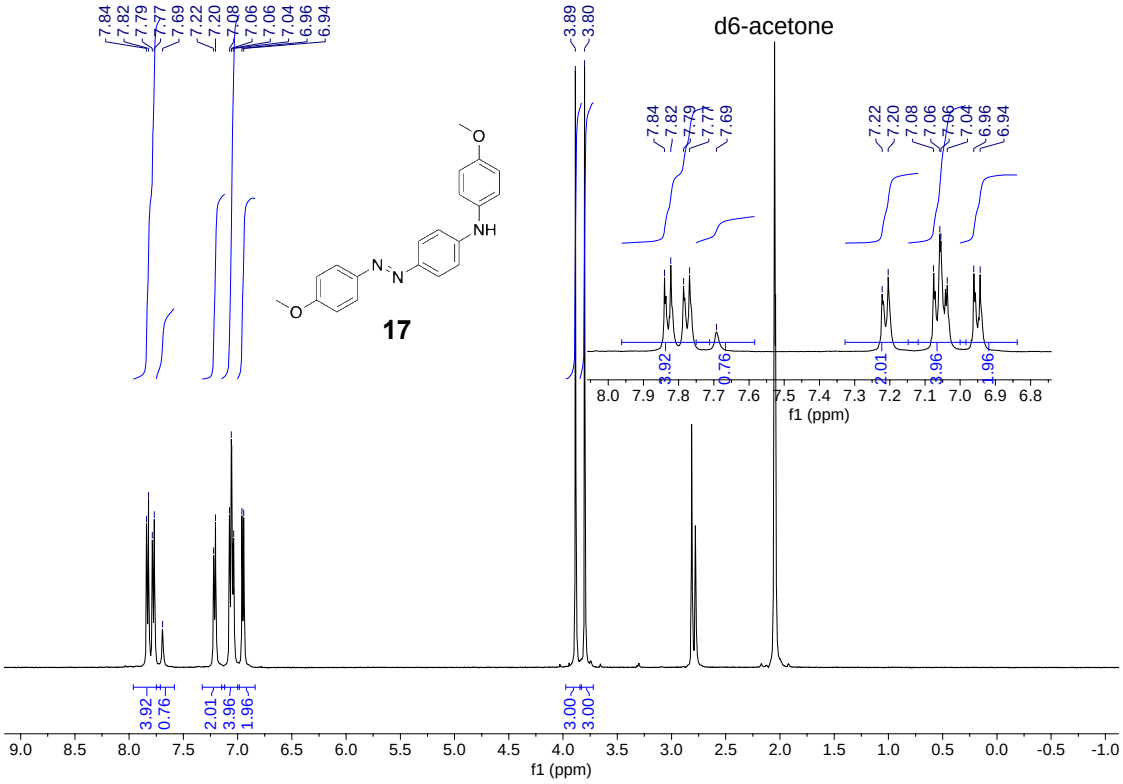

Figure S12. ^{1}H NMR spectrum (360 MHz) of **17** in d6-acetone

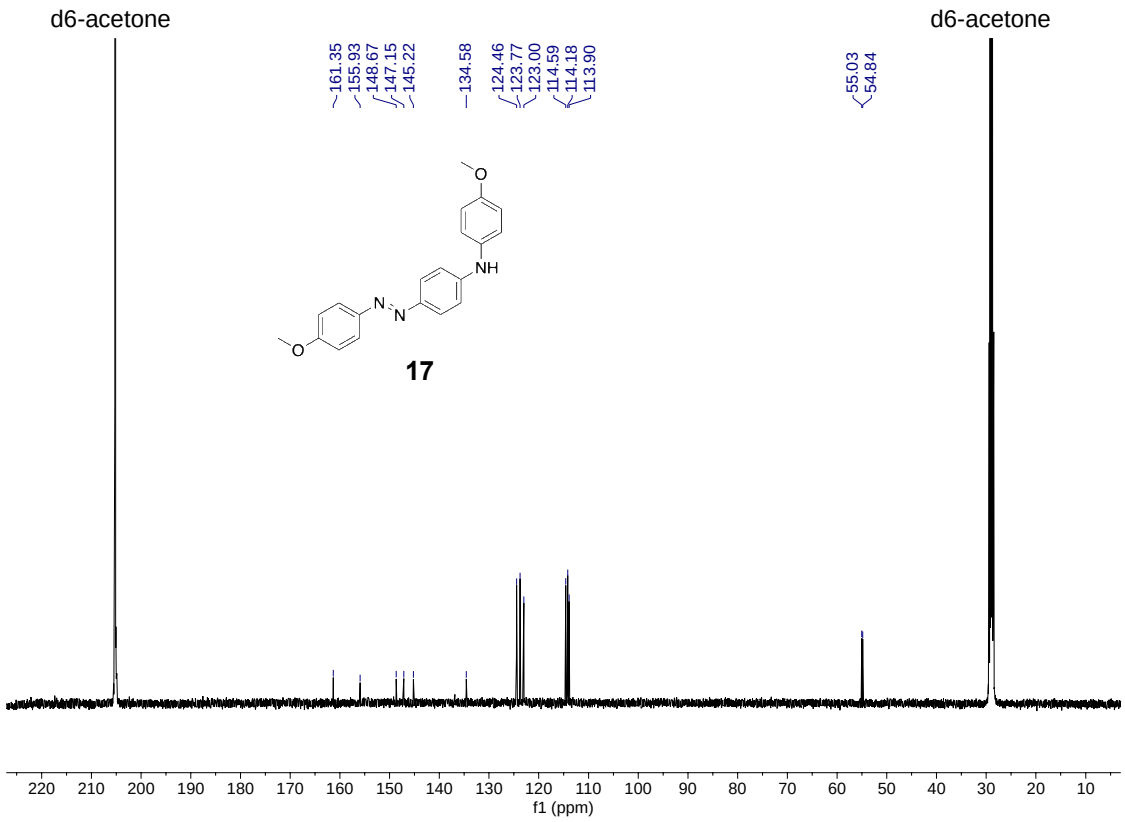

Figure S13. ^{13}C {^{1}H} NMR spectrum (125 MHz) of **17** in d6-acetone

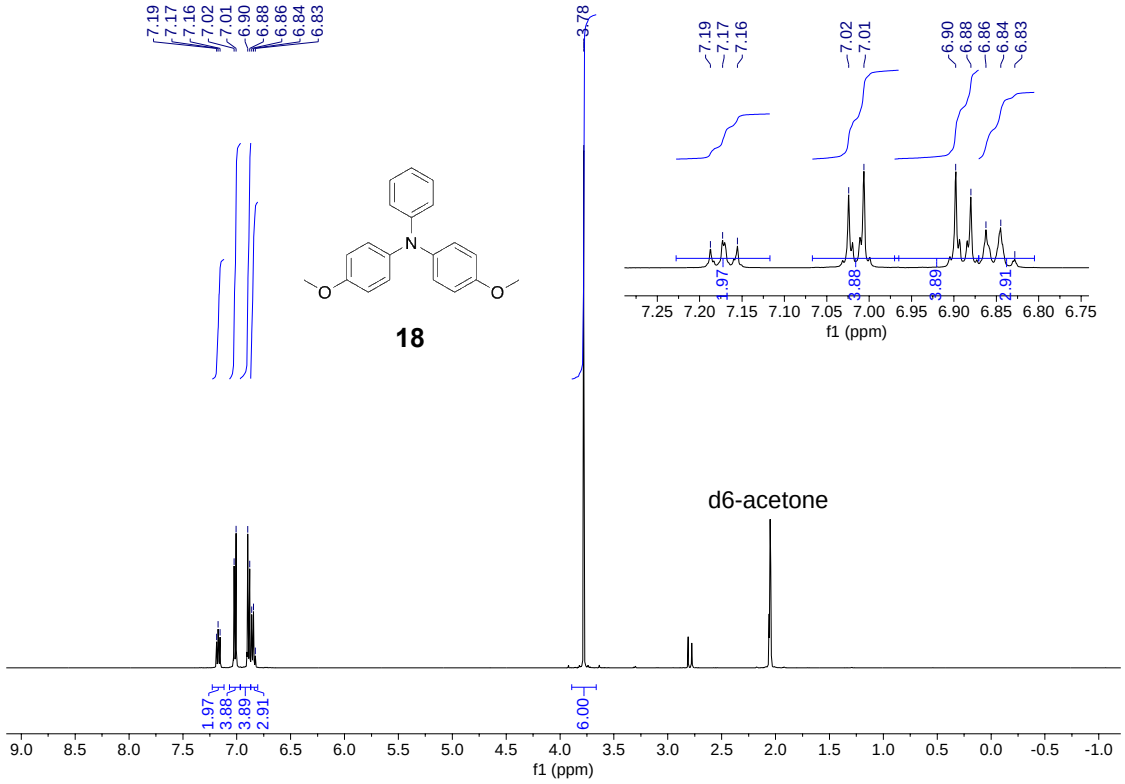

Figure S14. ^{1}H NMR spectrum (500 MHz) of **18** in d6-acetone

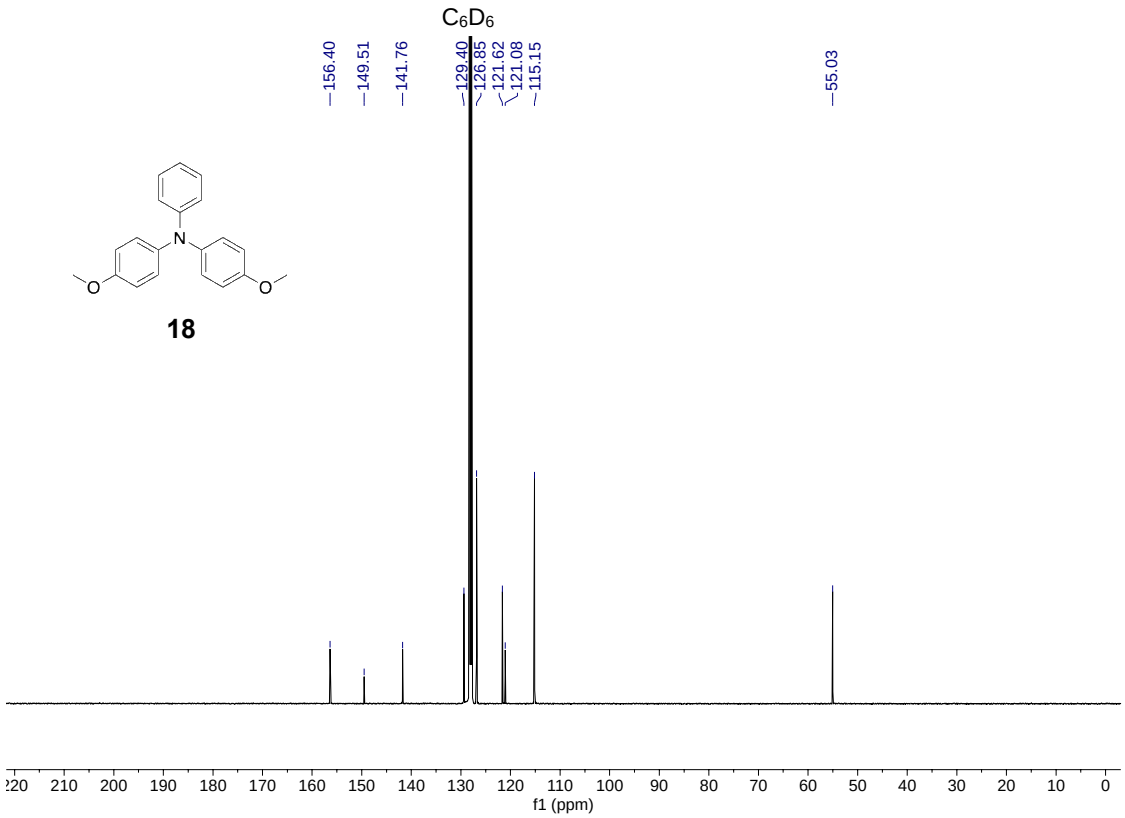

Figure S15. ^{13}C {^{1}H} NMR spectrum (125 MHz) of **18** in C_6D_6

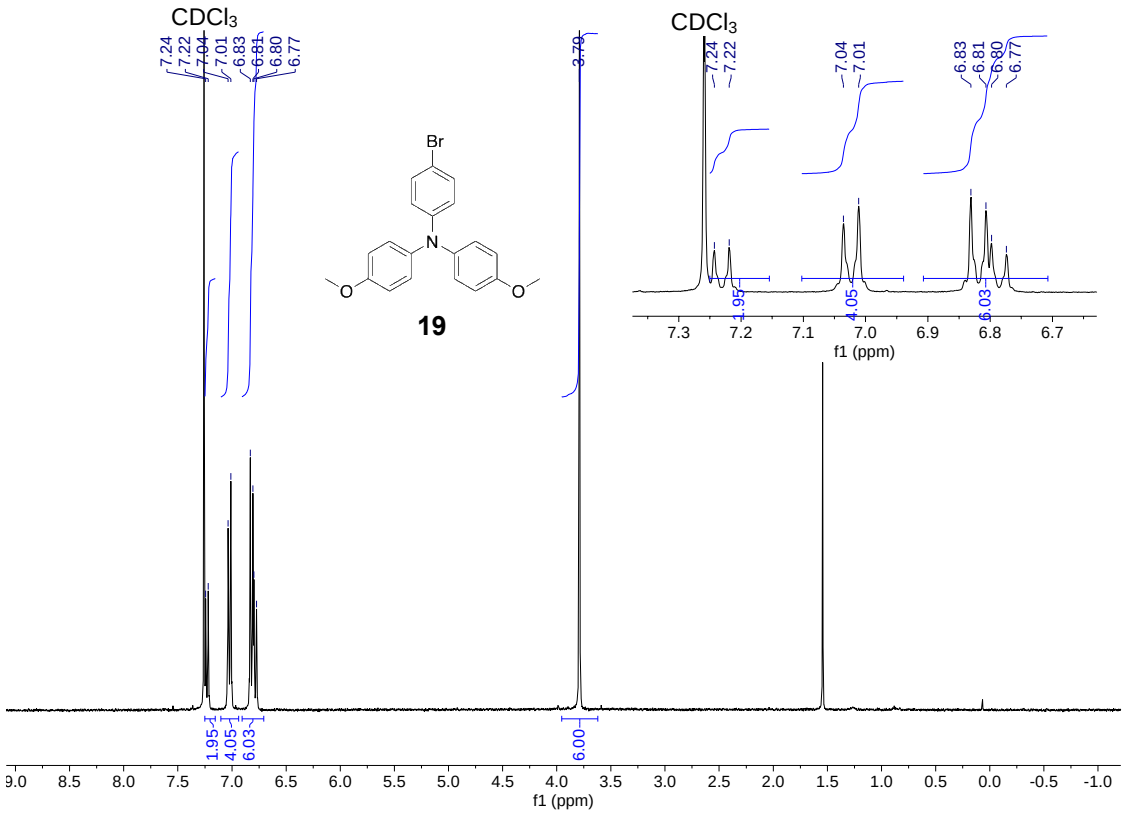

Figure S16. ^{1}H NMR spectrum (360 MHz) of **19** in $CDCl_3$

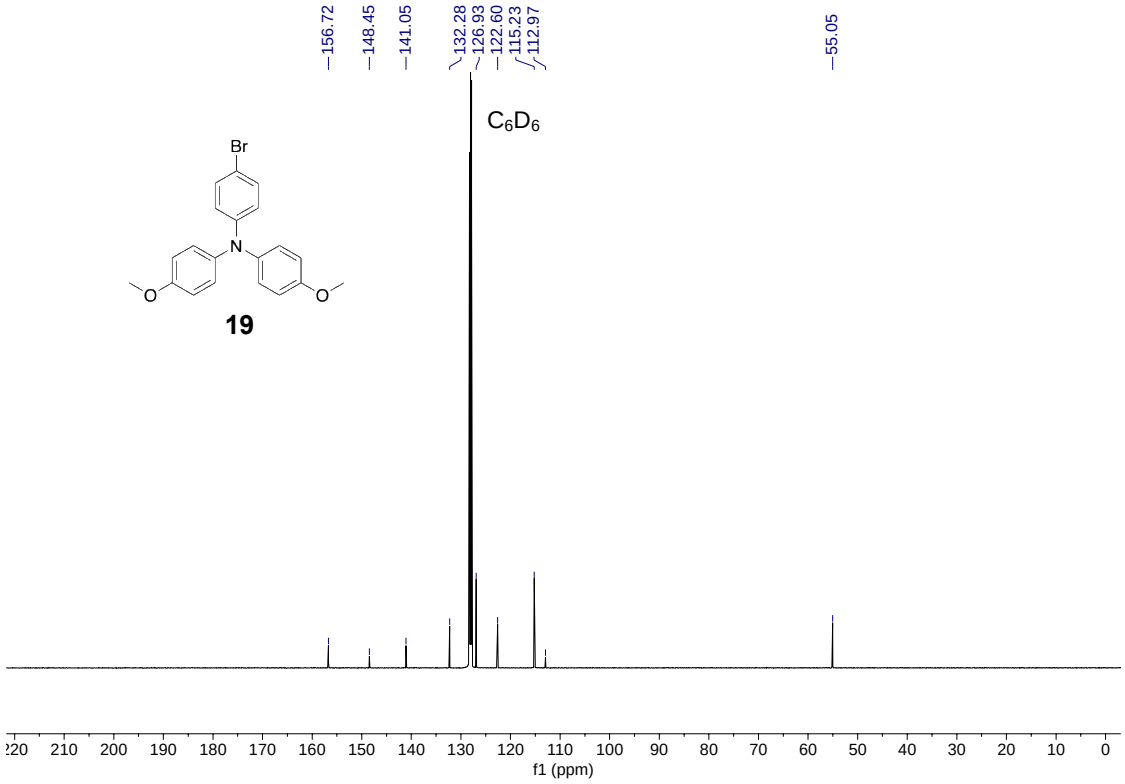

Figure S17. ^{13}C {^{1}H} NMR spectrum (125 MHz) of **19** in C_6D_6

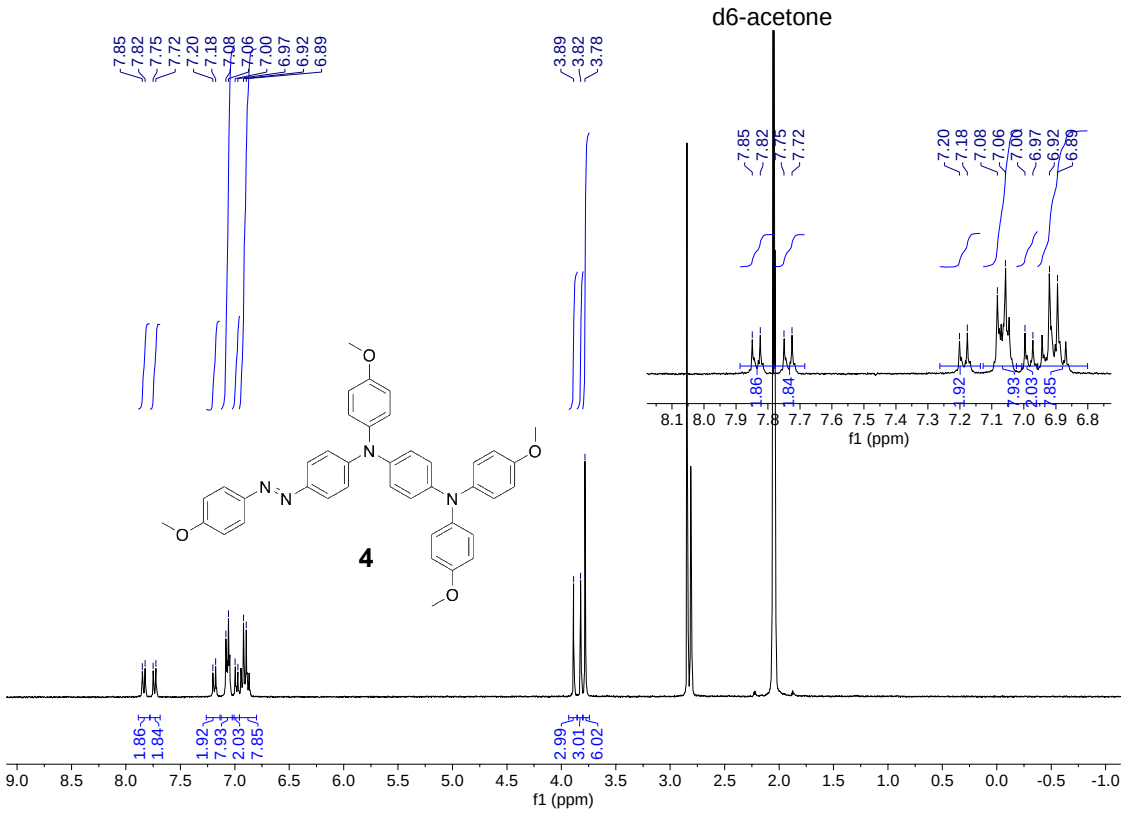

Figure S18. ^{1}H NMR spectrum (360 MHz) of **4** in d6-acetone

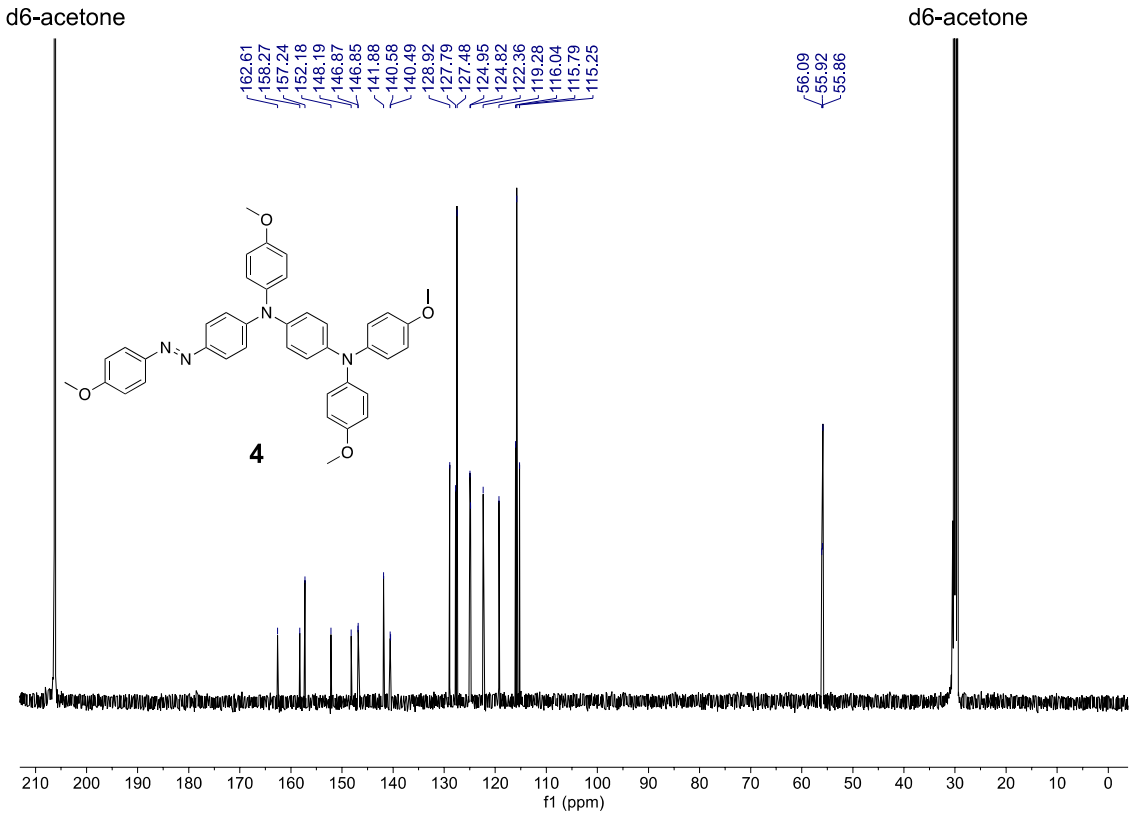

Figure S19. ^{13}C {^{1}H} NMR spectrum (125 MHz) of **4** in d6-acetone

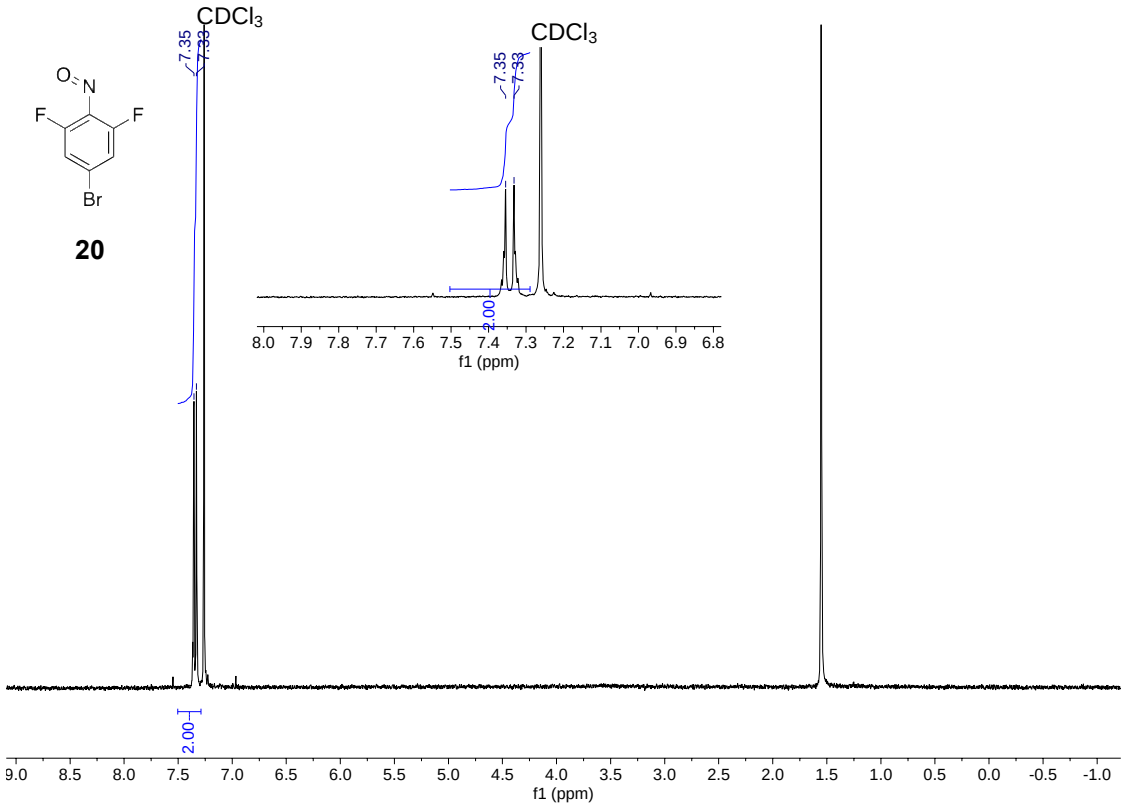

Figure S20. ^{1}H NMR spectrum (360 MHz) of **20** in $CDCl_3$

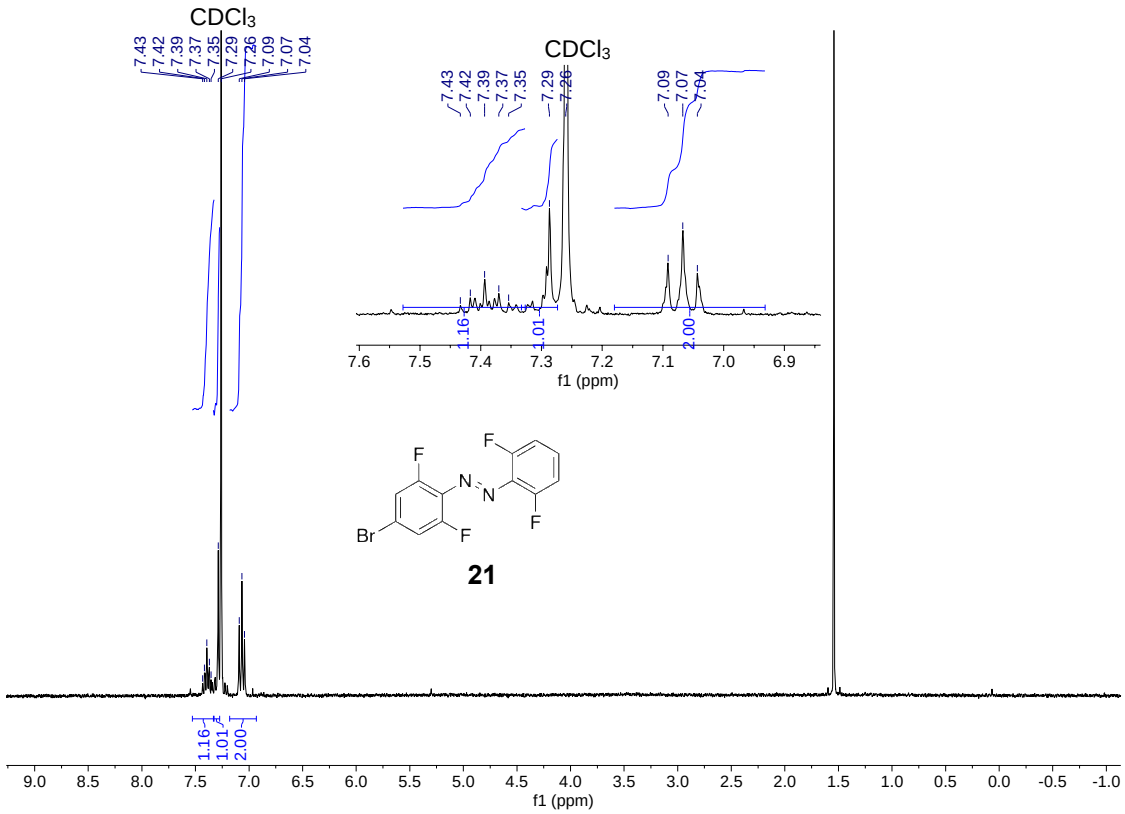

Figure S21. ^{1}H NMR spectrum (360 MHz) of **21** in $CDCl_3$

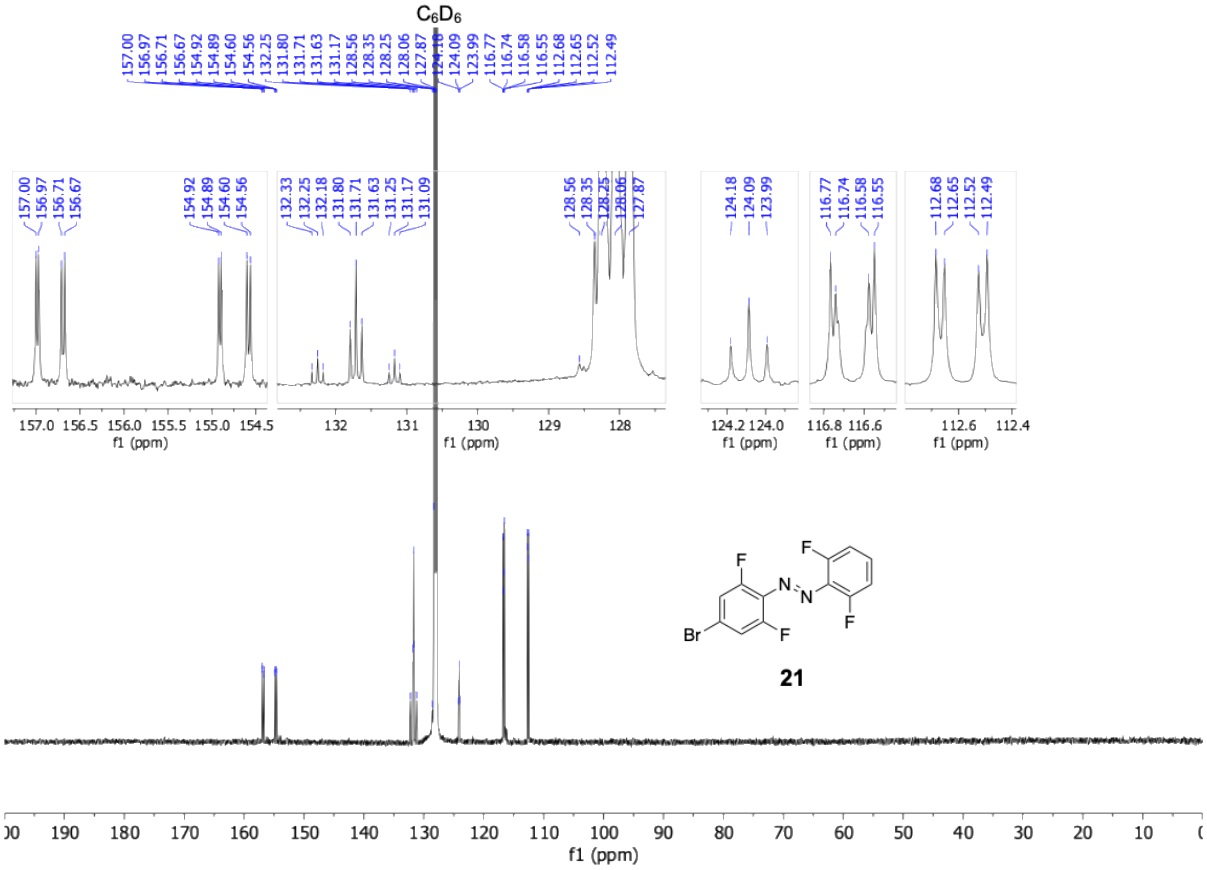

Figure S22. ^{13}C {^{1}H} NMR spectrum (125 MHz) of **21** in C_6D_6

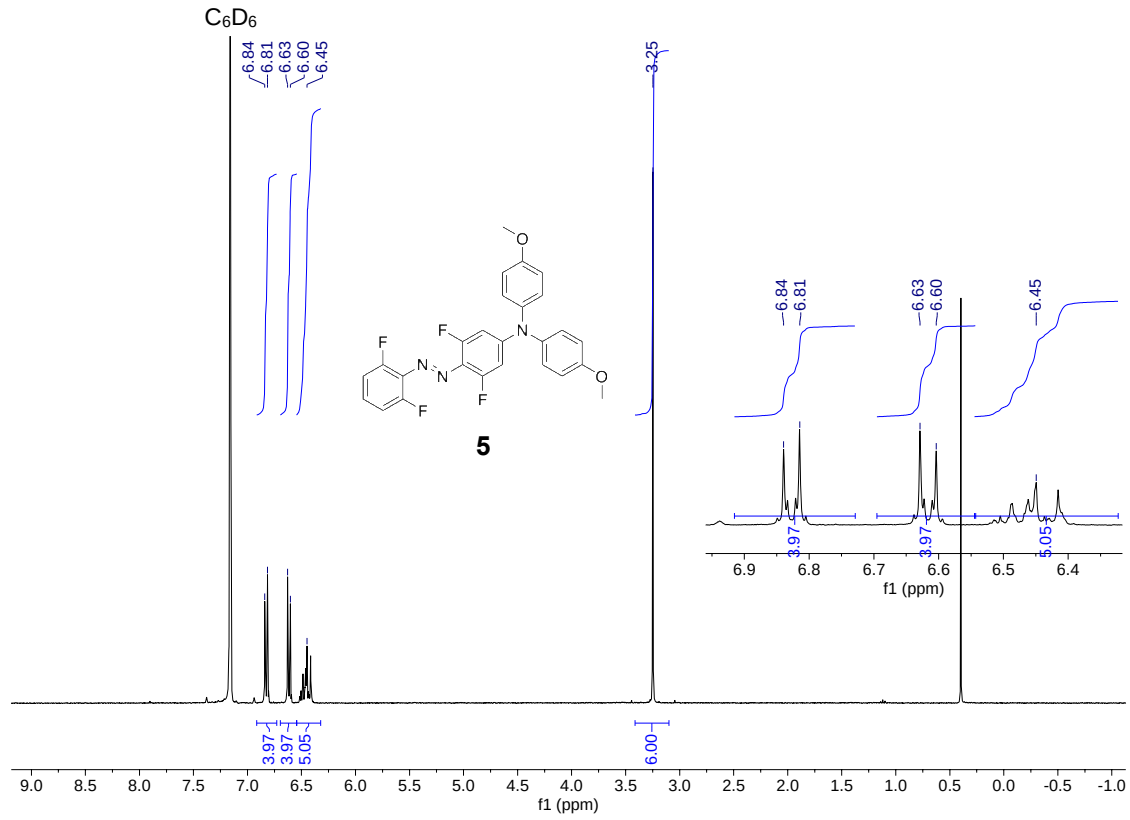

Figure S23. ^{1}H NMR spectrum (360 MHz) of **5** in C_6D_6

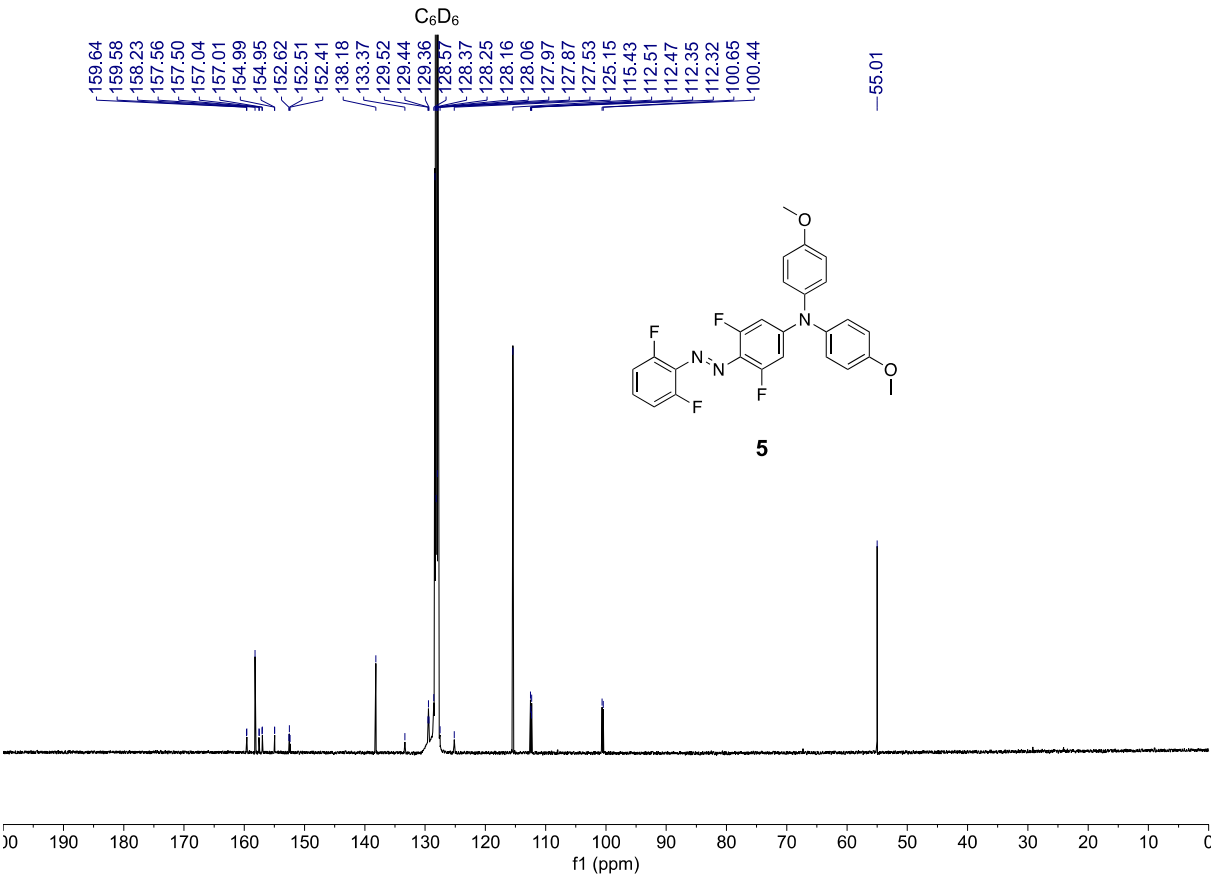

Figure S24. ^{13}C {^{1}H} NMR spectrum (125 MHz) of **5** in C_6D_6

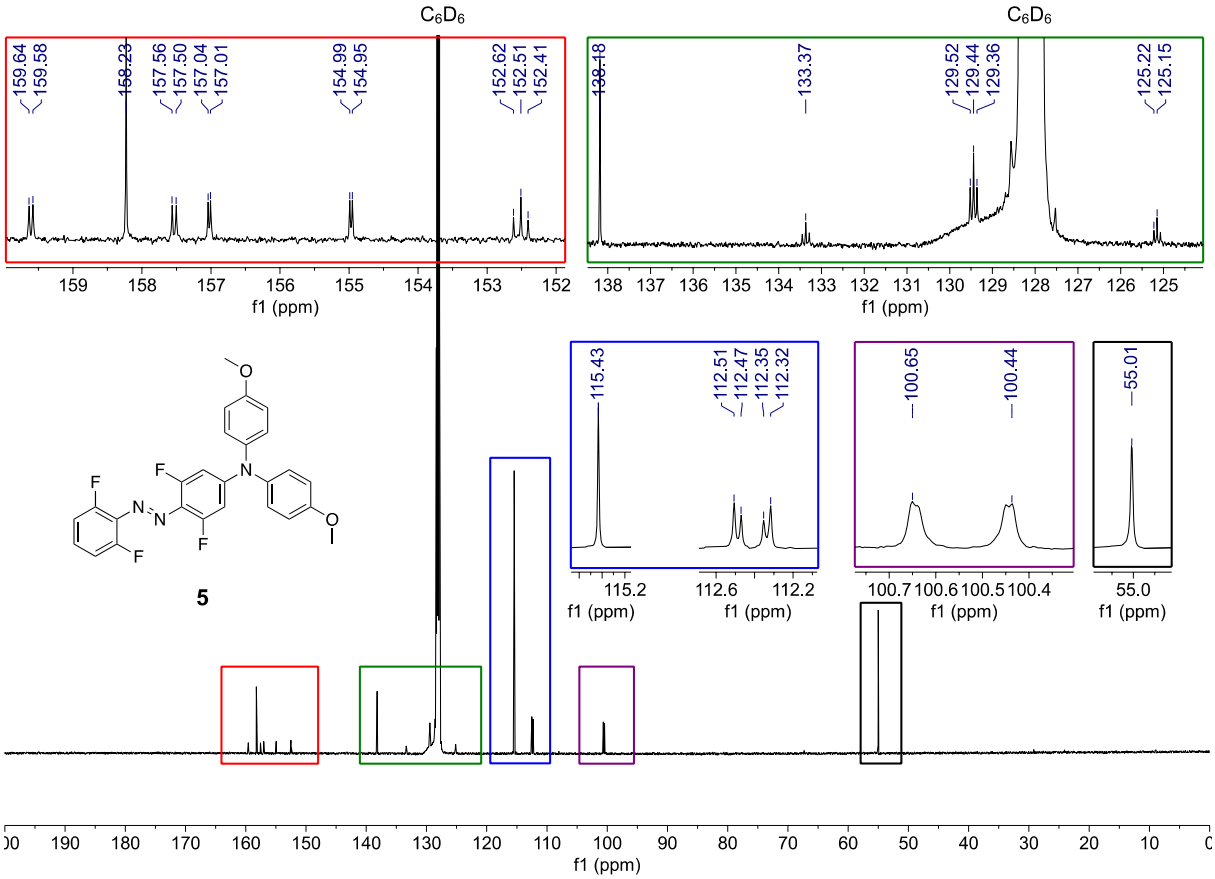

Figure S25. ^{13}C {^{1}H} NMR spectrum (125 MHz) of **5** in C_6D_6 with various expansions of peaks and regions of the spectrum

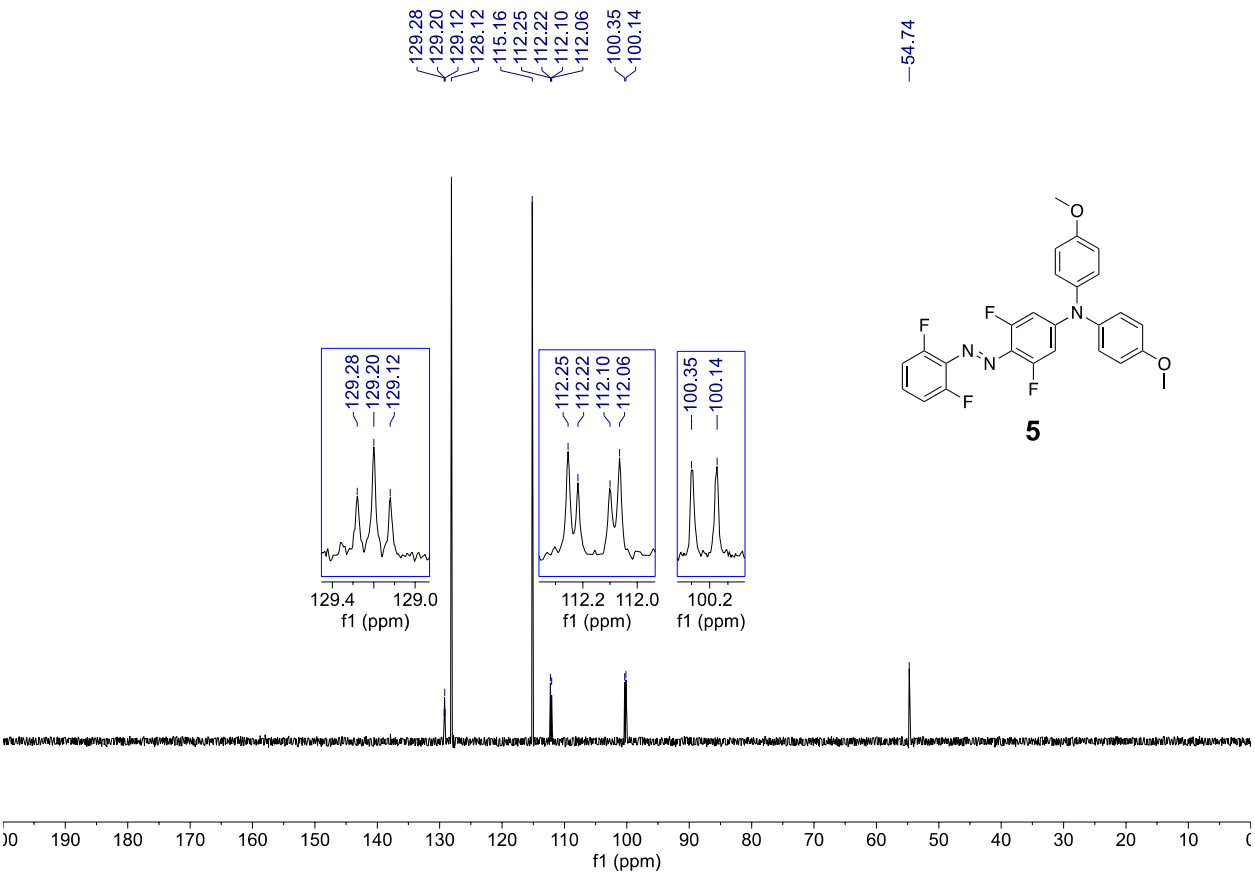

Figure S26. DEPT135 ^{13}C {^{1}H} NMR spectrum (125 MHz) of **5** in C_6D_6

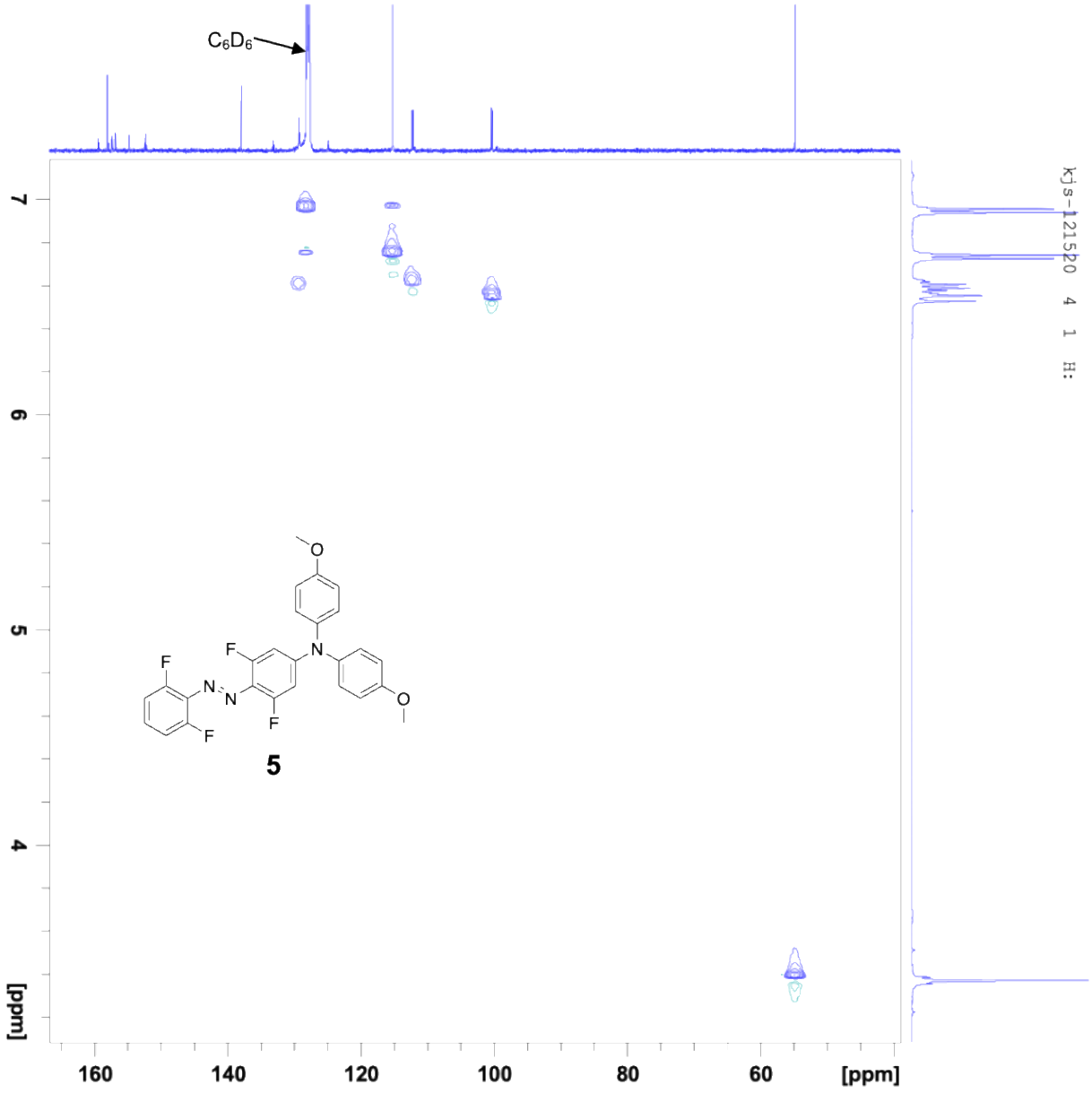

Figure S27. ^{1}H-^{13}C HSQC NMR spectrum (500 MHz (^{1}H)/125 MHz (^{13}C)) of **5** in C_6D_6

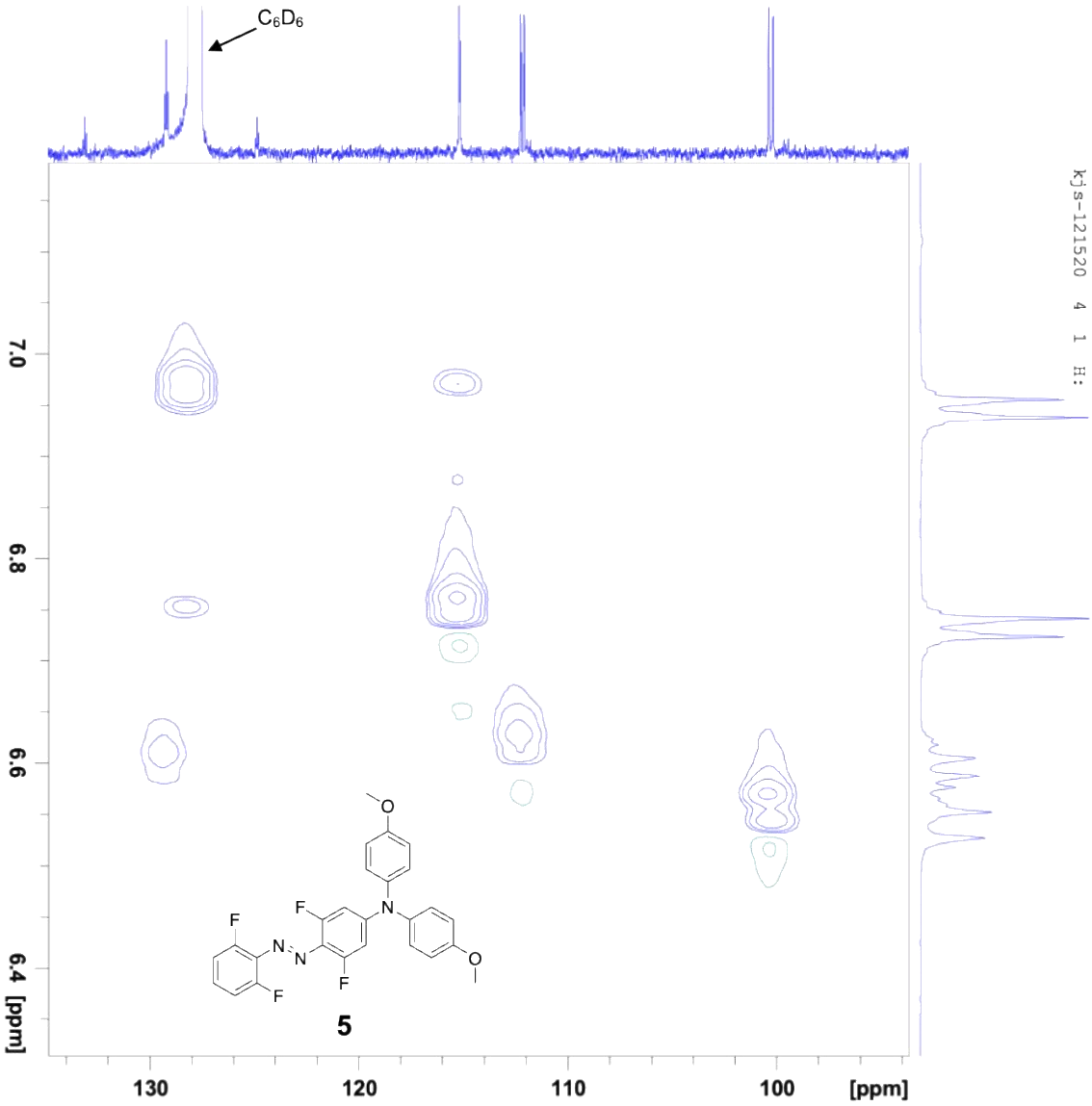

Figure S28. Expansion of aromatic region of ^{1}H-^{13}C HSQC NMR spectrum (500 MHz (^{1}H)/125 MHz (^{13}C)) of **5** in C_6D_6

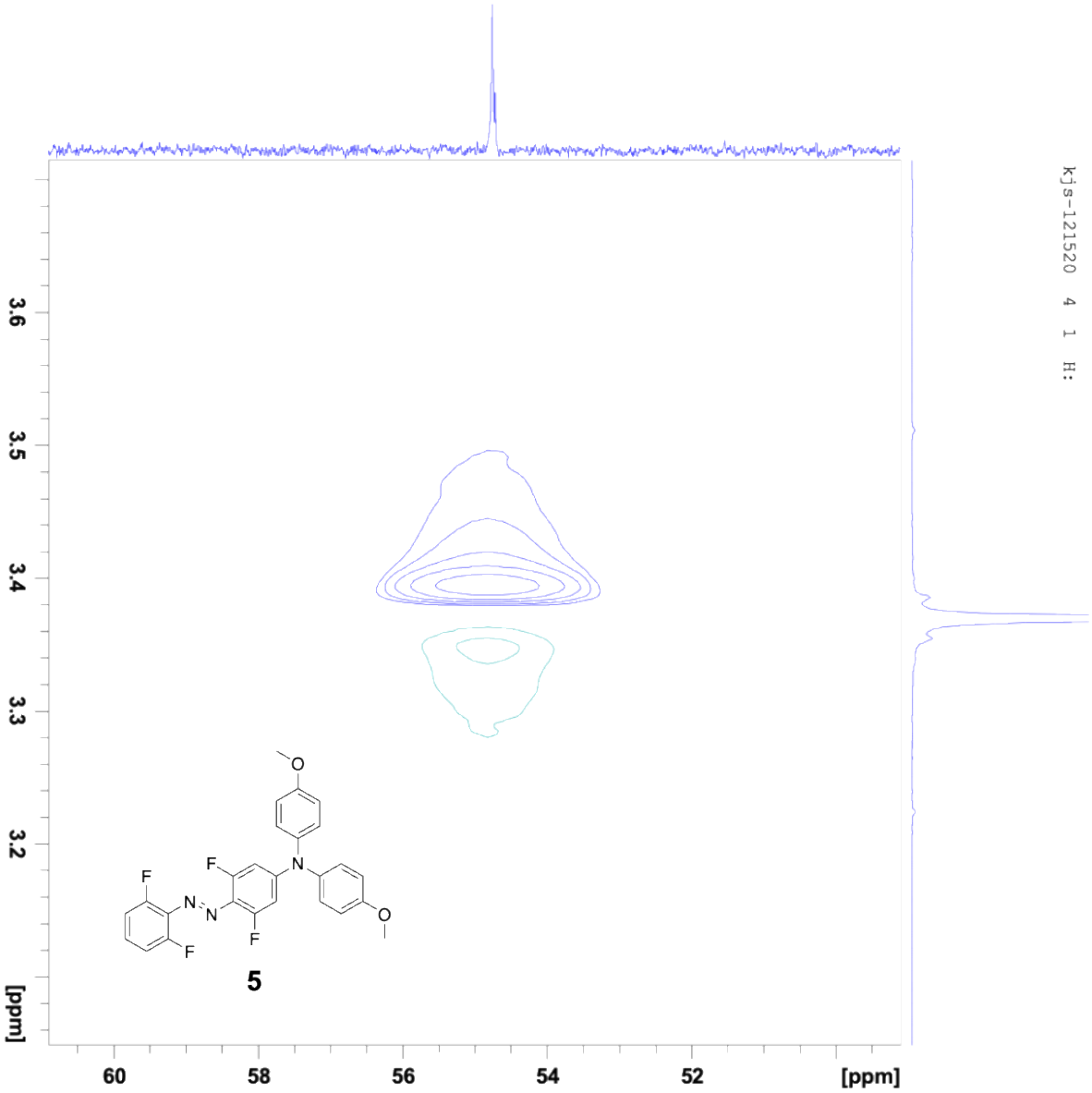

Figure S29. Expansion of methoxy region of ^{1}H-^{13}C HSQC NMR spectrum (500 MHz (^{1}H)/125 MHz (^{13}C)) of **5** in C_6D_6

2. UV-vis spectrum of $4^{\bullet+}PF_6^-$

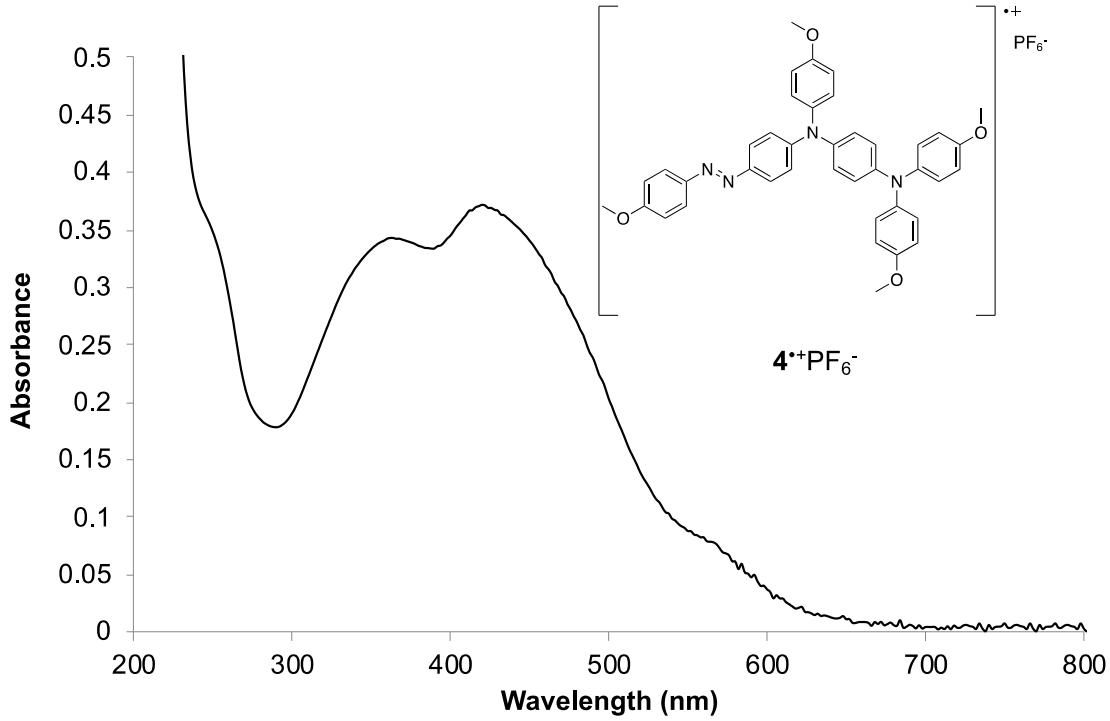

Figure S30. Optical spectrum of $\mathbf{4}^{\bullet+}PF_6^-$ (1.9 x 10^{-4} M) in $CHCl_3$ in a 1.0 cm quartz cuvette at 295 K. λ_{max} = 420 nm; ε_{420} = 2,000 $M^{-1}cm^{-1}$

3. *E*→*Z* photoisomerization of 2-5 followed by UV-vis spectroscopy

LED source (nm)	Full width at half maximum (nm)	Wavelength of highest intensity emission (nm)
395-410	14 (401-415)	408
430	16 (418-434)	426

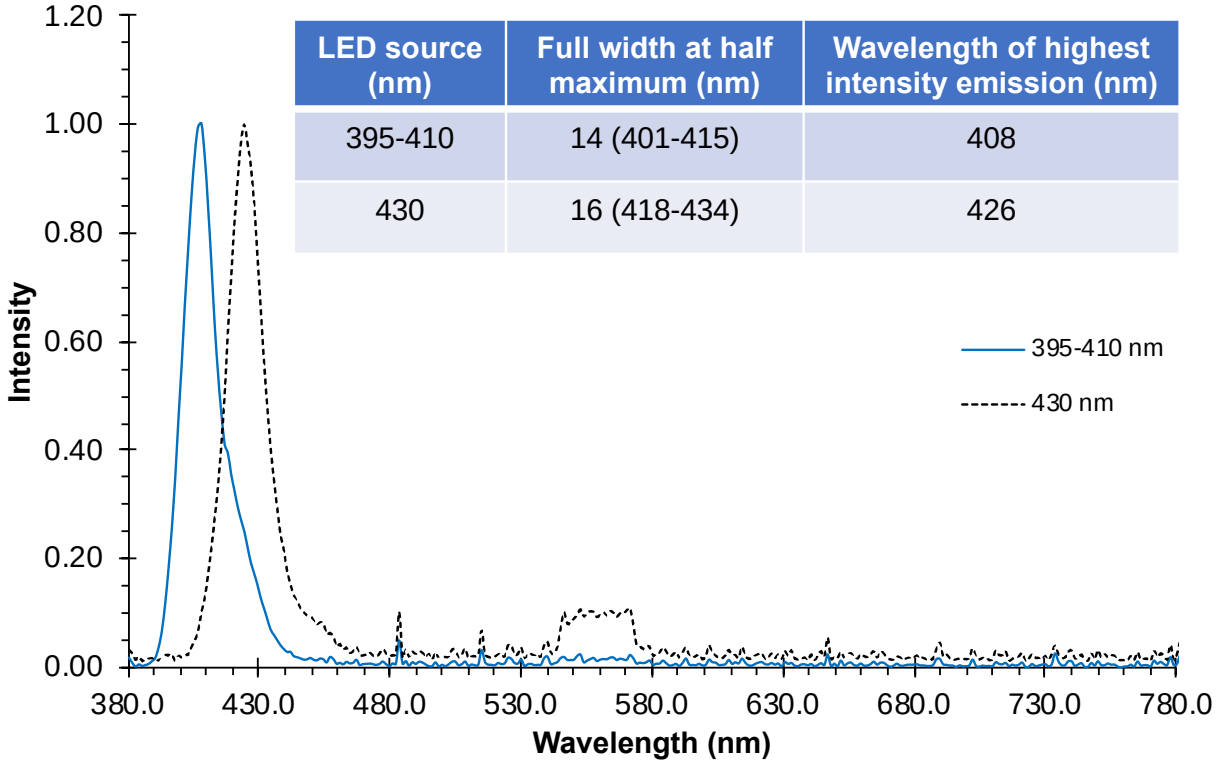

Figure S31. Excitation spectra for the 395-410 nm (7 W) and 430 nm LED (7 W) irradiation sources used to induce *E*→*Z* isomerization.

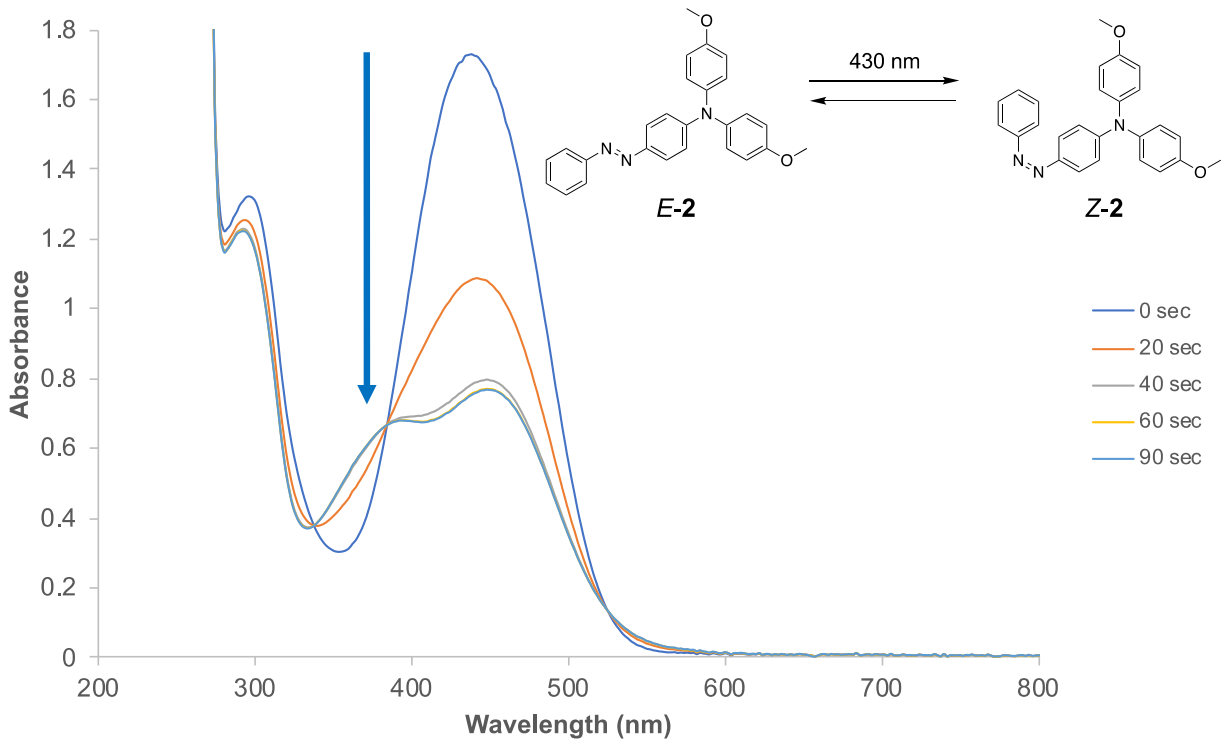

Figure S32. Overlay of optical spectra of **2** (6.35 x 10^{-4} M in deaerated C_6D_6 in a 0.1 cm quartz cuvette) recorded at different times during the *E*-**2**→*Z*-**2** photoisomerization process occurring in response to 430 nm irradiation at 295 K.

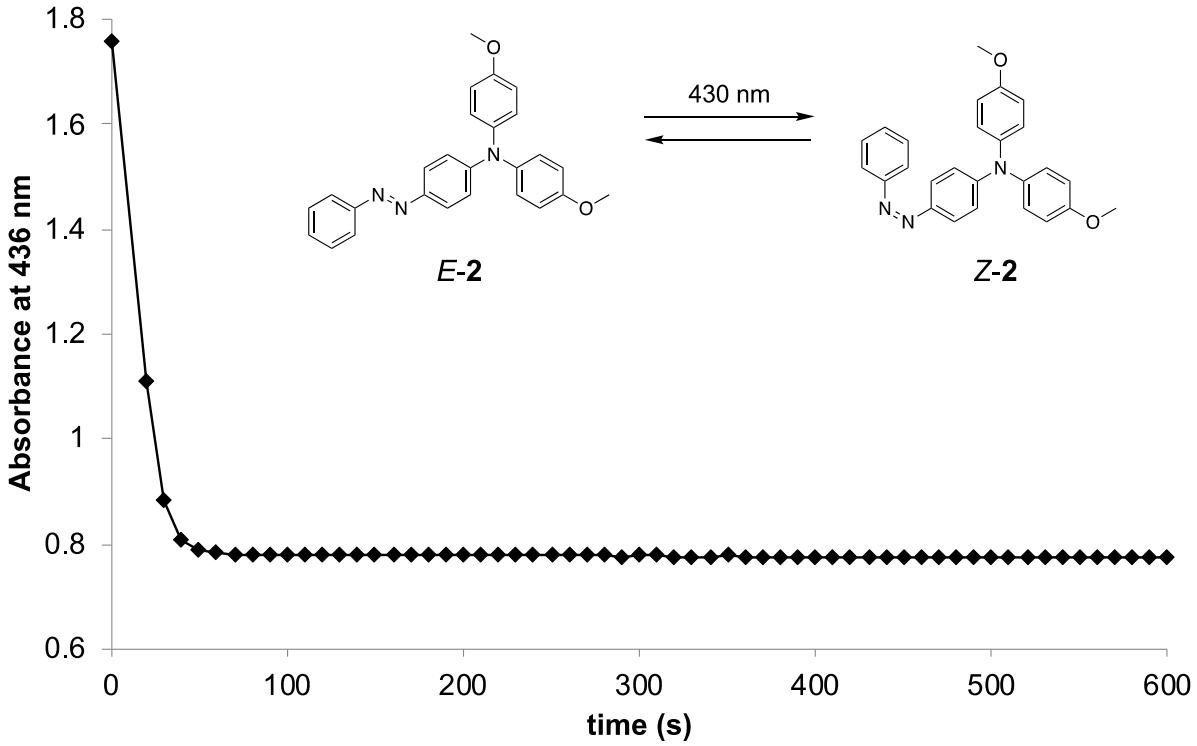

Figure S33. Time radiation profile indicating *E*→*Z* photoisomerization of **2** (6.35 x 10^{-4} M in deaerated C_6D_6 in a 0.1 cm quartz cuvette) that occurs upon 430 nm LED irradiation at 295 K.

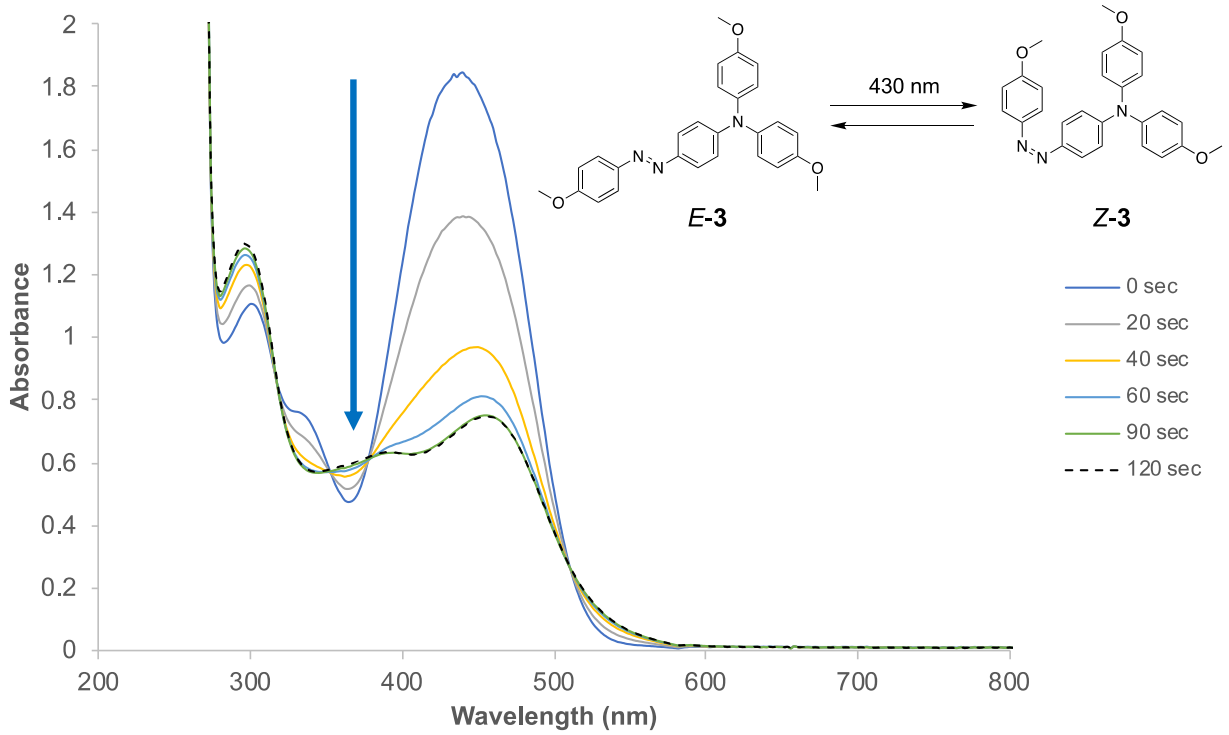

Figure S34. Overlay of optical spectra of **3** (6.37 x 10^{-4} M in deaerated C_6D_6 in a 0.1 cm quartz cuvette) recorded at different times during the *E*-**3**→*Z*-**3** photoisomerization process that occurs in response to 430 nm irradiation at 295 K.

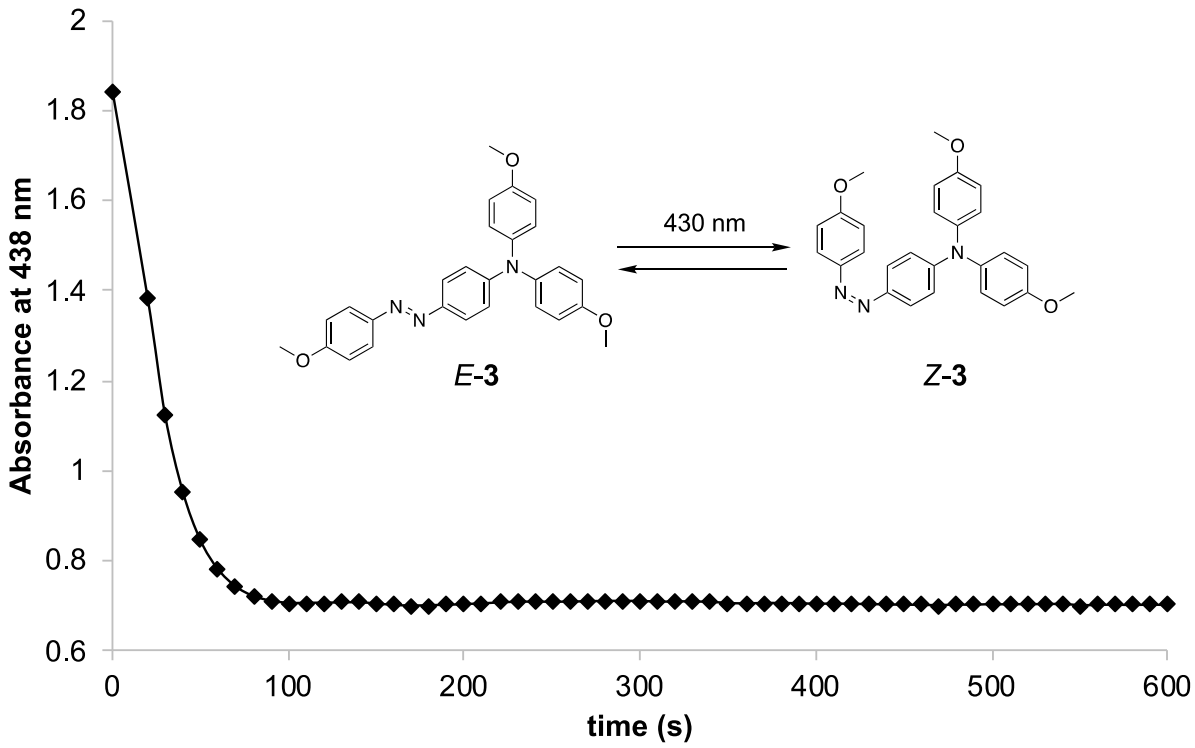

Figure S35. Time radiation profile following absorbance at 438 nm for a solution of **3** in deaerated C_6D_6 (6.37 x 10^{-4} M in a 0.1 cm quartz cuvette) during the *E*-**3**→*Z*-**3** photoisomerization process that occurs in response to 430 nm LED irradiation at 295 K.

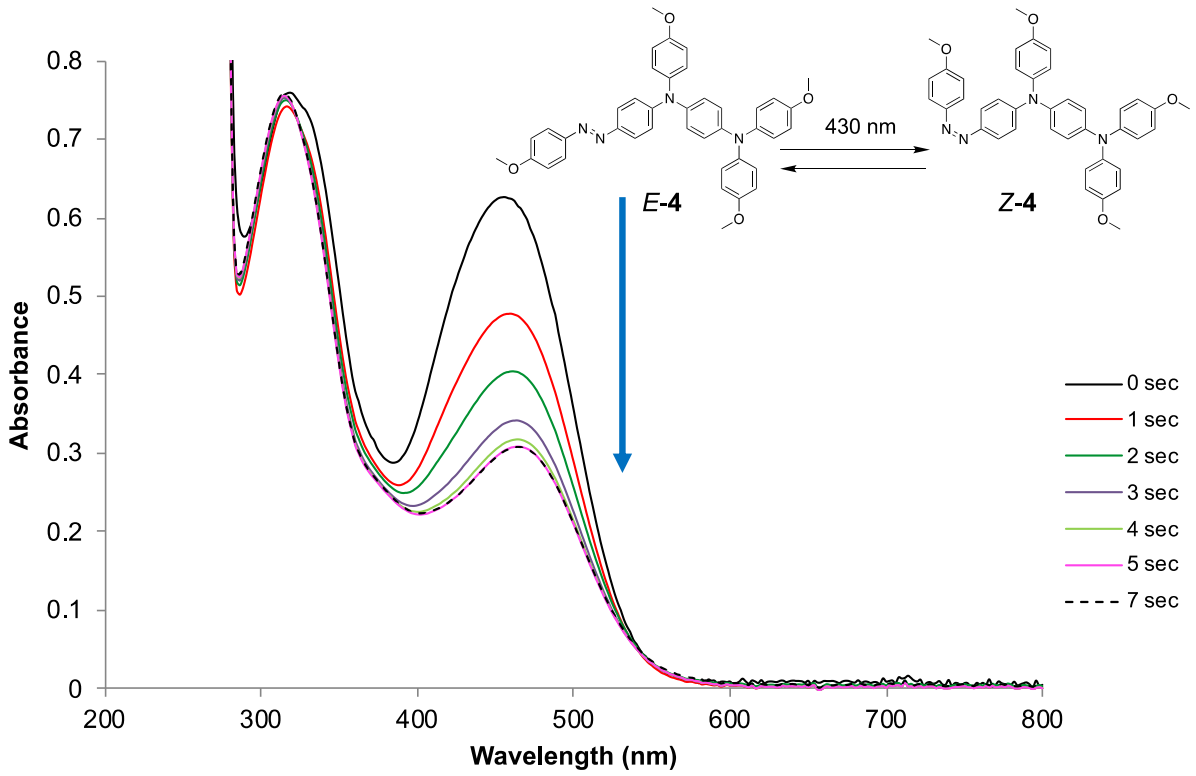

Figure S36. Overlay of optical spectra of **4** (3.14×10^{-4} M in deaerated benzene in a 0.1 cm quartz cuvette) recorded at different times during the *E*-**4**→*Z*-**4** photoisomerization process that occurs in response to 430 nm irradiation at 295 K.

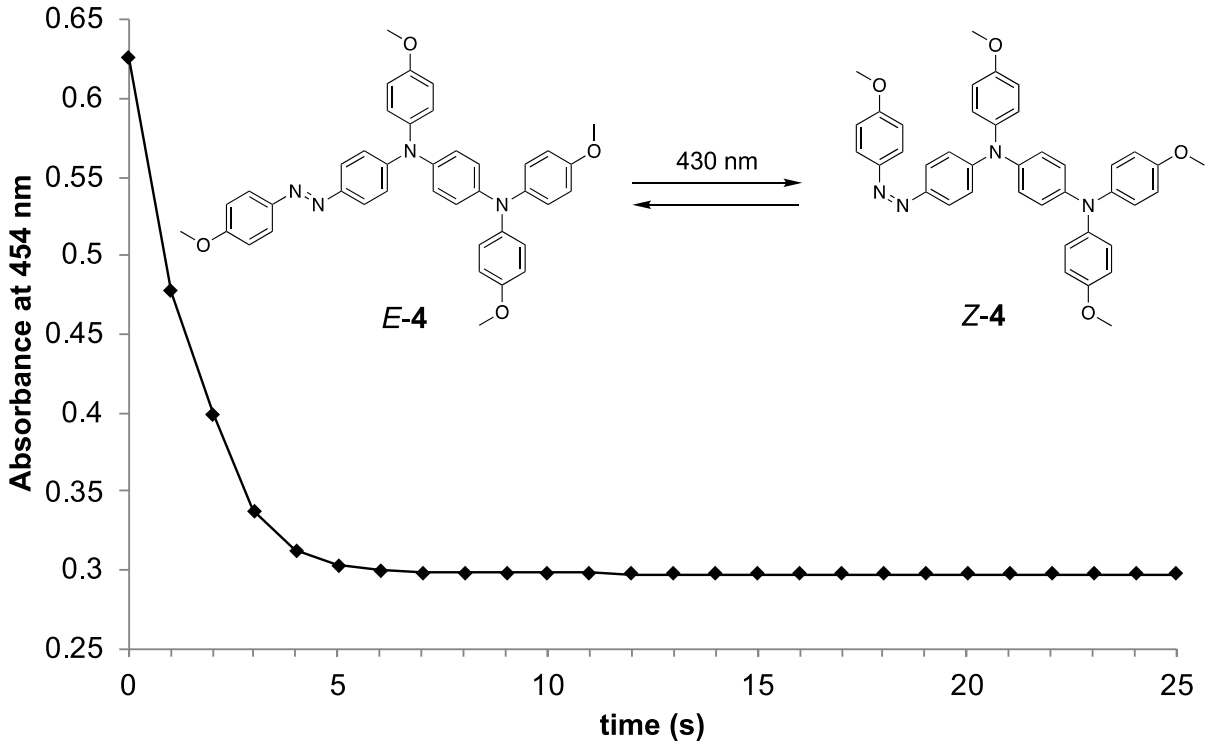

Figure S37. Time radiation profile following absorbance at 454 nm for a solution of **4** in deaerated benzene (3.14×10^{-4} M in a 0.1 cm quartz cuvette) during the *E*-**4**→*Z*-**4** photoisomerization process that occurs in response to 430 nm LED irradiation at 295 K.

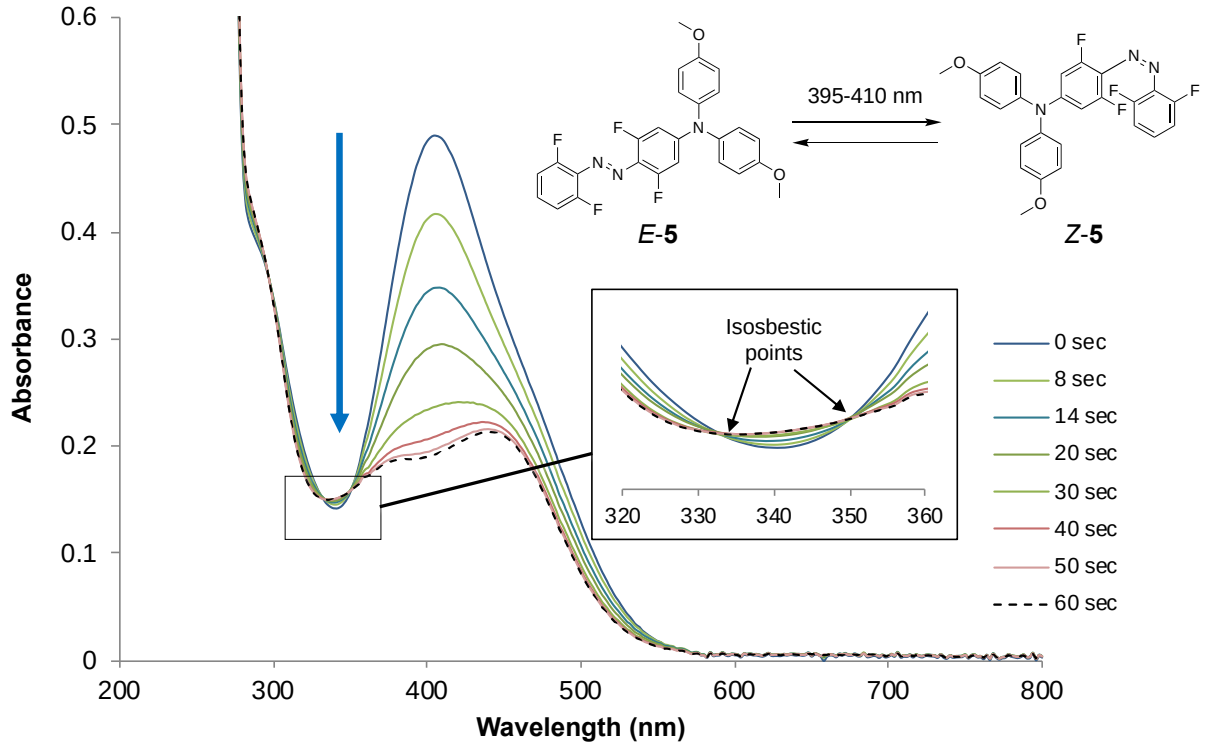

Figure S38. Overlay of optical spectra of **5** (1.8 x 10^{-4} M in deaerated benzene in a 0.1 cm quartz cuvette) recorded at different times during the *E*-**5**→*Z*-**5** photoisomerization process that occurs in response to 395-410 nm irradiation at 295 K.

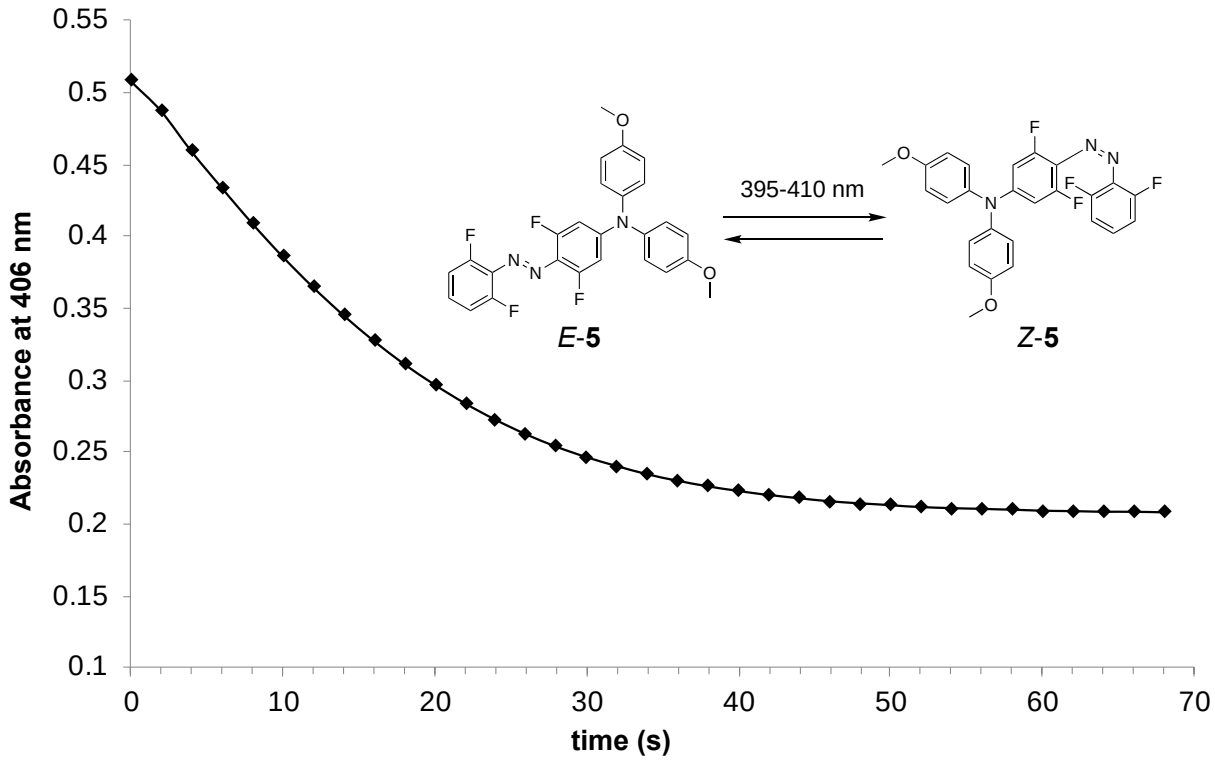

Figure S39. Time radiation profile following absorbance at 406 nm for a solution of **5** in deaerated benzene (1.8×10^{-4} M in a 0.1 cm quartz cuvette) during the *E*-**5**→*Z*-**5** photoisomerization process that occurs in response to 395-410 nm LED irradiation at 295 K.

4. Determination of photostationary state *Z*/*E* ratios for 2-5 by ^{1}H NMR spectroscopy

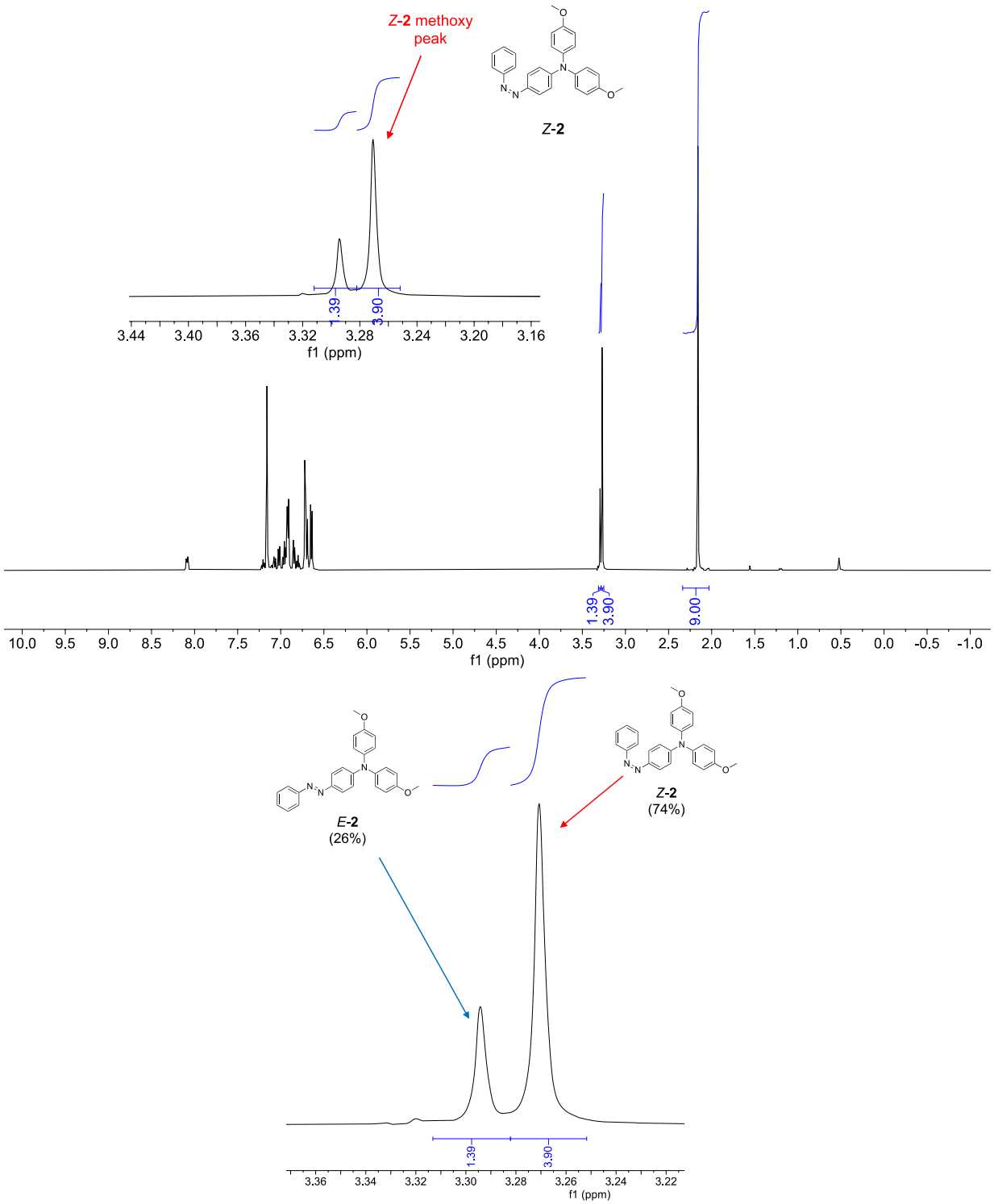

Figure S40. (top) Full spectrum view of the ^{1}H NMR spectrum (500 MHz) of the mixture of *E*-**2** and *Z*-**2** ([**2**] = 4.39 x 10^{-2} M in C_6D_6) at the 430 nm PSS. (bottom) Expanded view of the methoxy section of the ^{1}H NMR spectrum of the *E*-**2**/*Z*-**2** mixture at the 430 nm PSS. Integrating

the *E* and *Z* methoxy peaks indicated 74% *Z* content at the 430 nm PSS in C_6D_6. (2.0 µL mesitylene was present as an internal standard; 7 W LED 430 nm irradiation source)

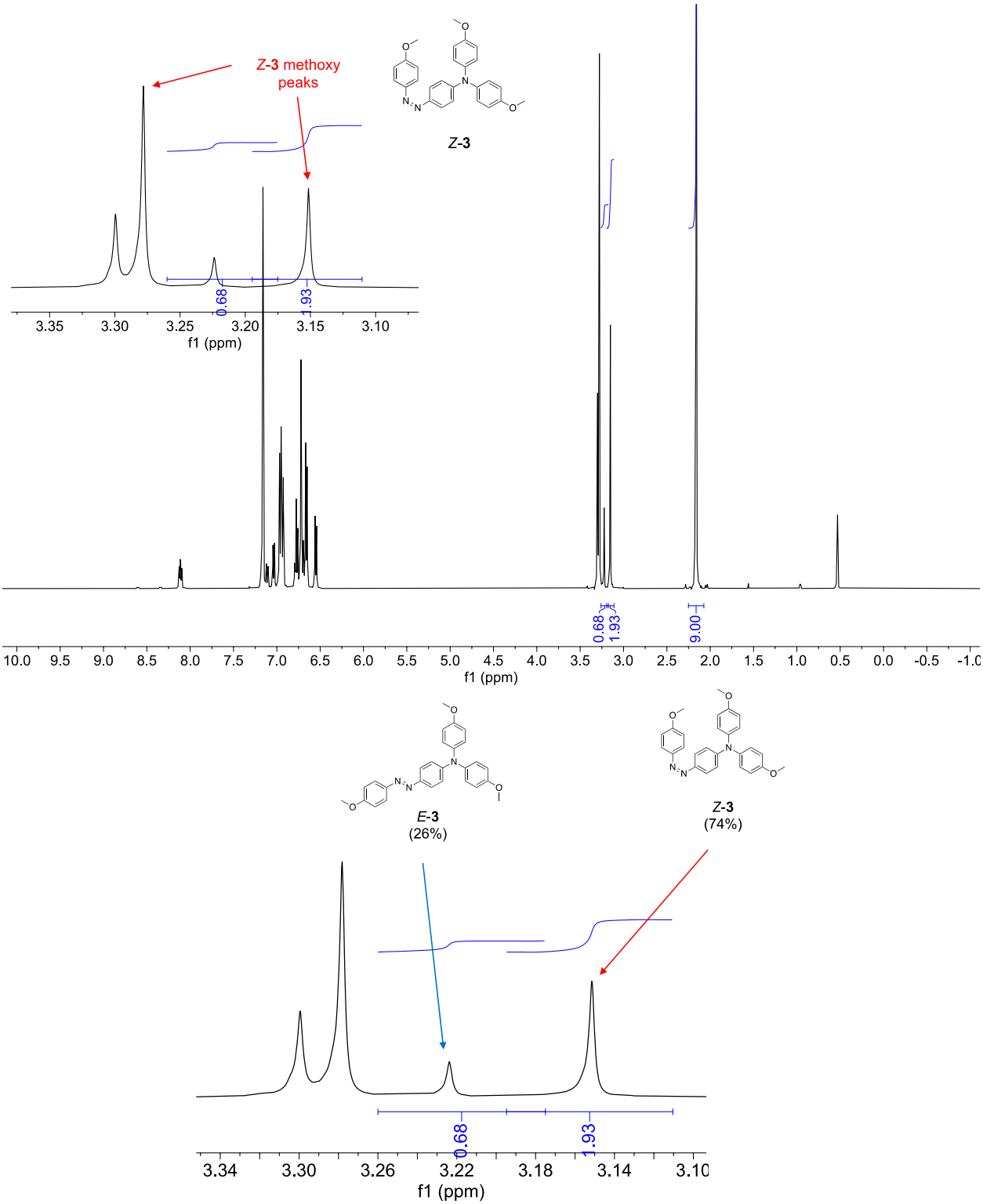

Figure S41. (top) Full spectrum view of the ^{1}H NMR spectrum (500 MHz) of the mixture of *E*-**3** and *Z*-**3** ([**3**] = 3.82 x 10^{-2} M in C_6D_6) at the 430 nm PSS. (bottom) Expanded view of the

methoxy section of the ^{1}H NMR spectrum of the *E*-**3**/*Z*-**3** mixture at the 430 nm PSS. Integrating the *E* and *Z* methoxy peaks indicated 74% *Z* content at the 430 nm PSS in C_6D_6. (2.0 µL mesitylene was present as an internal standard; 7 W LED 430 nm irradiation source)

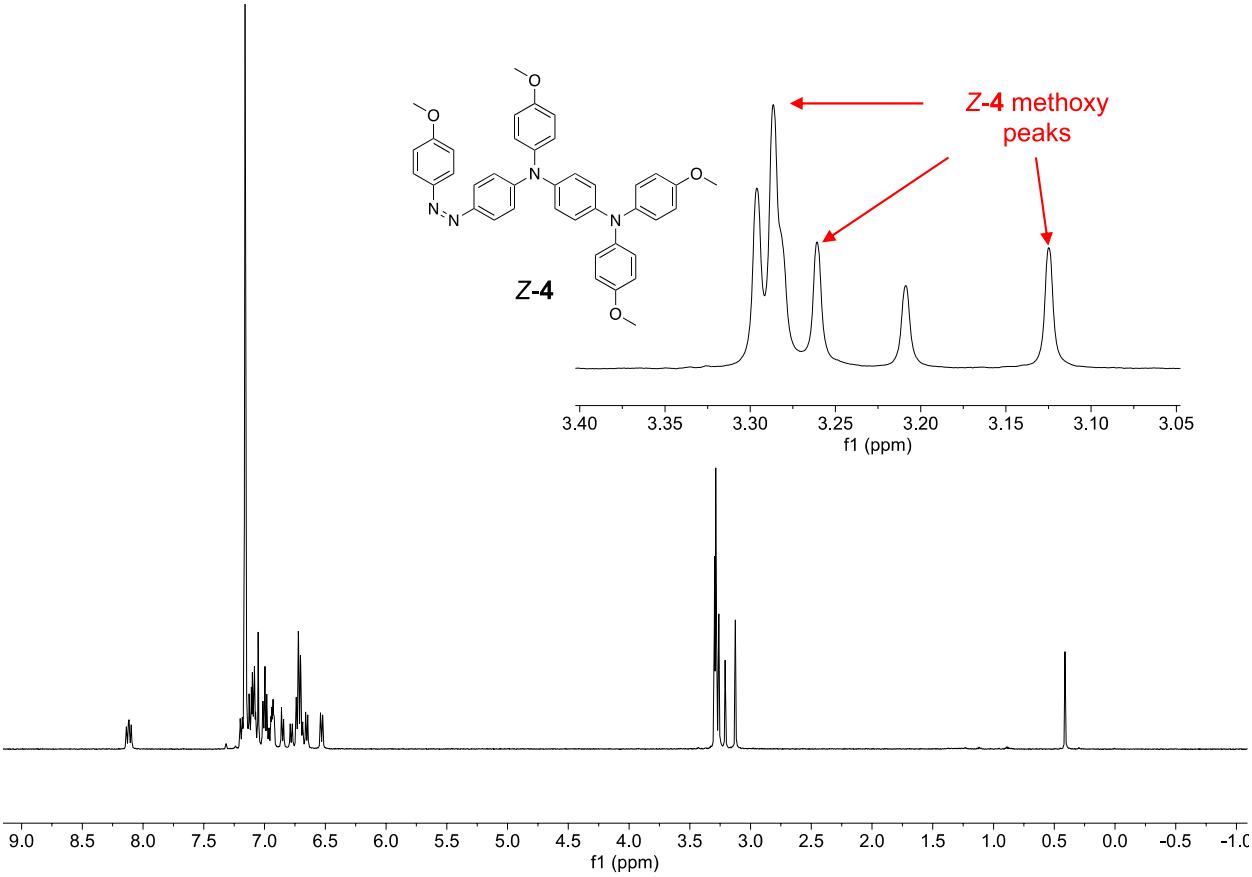

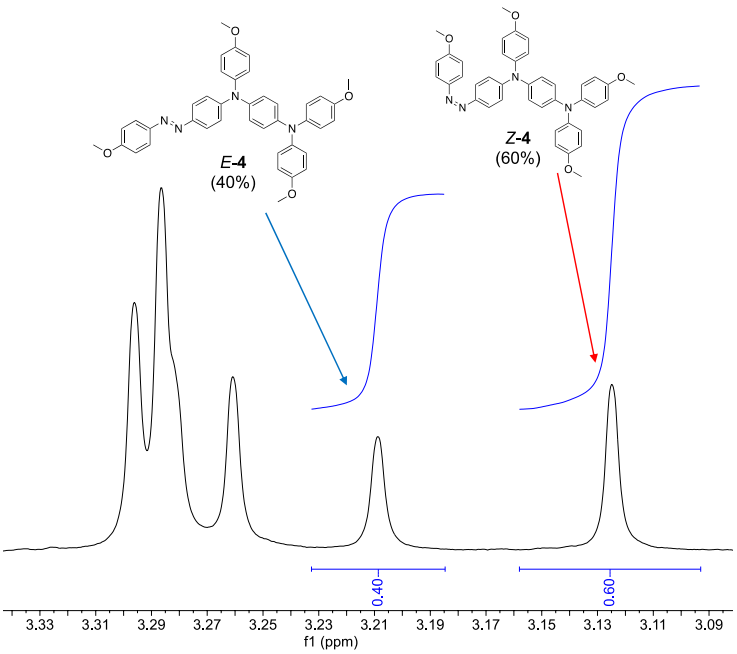

Figure S42. (top) Full spectrum view of the ^{1}H NMR spectrum (500 MHz) of the mixture of *E*-**4** and *Z*-**4** ([**4**] = 1.71 x 10^{-2} M in C_6D_6) at the 430 nm PSS. (bottom) Expanded view of the methoxy section of the ^{1}H NMR spectrum of the *E*-**4**/*Z*-**4** mixture at the 430 nm PSS. Integrating the *E* and *Z* methoxy peaks indicated 60% *Z* content at the 430 nm PSS in C_6D_6. (7 W LED 430 nm irradiation source)

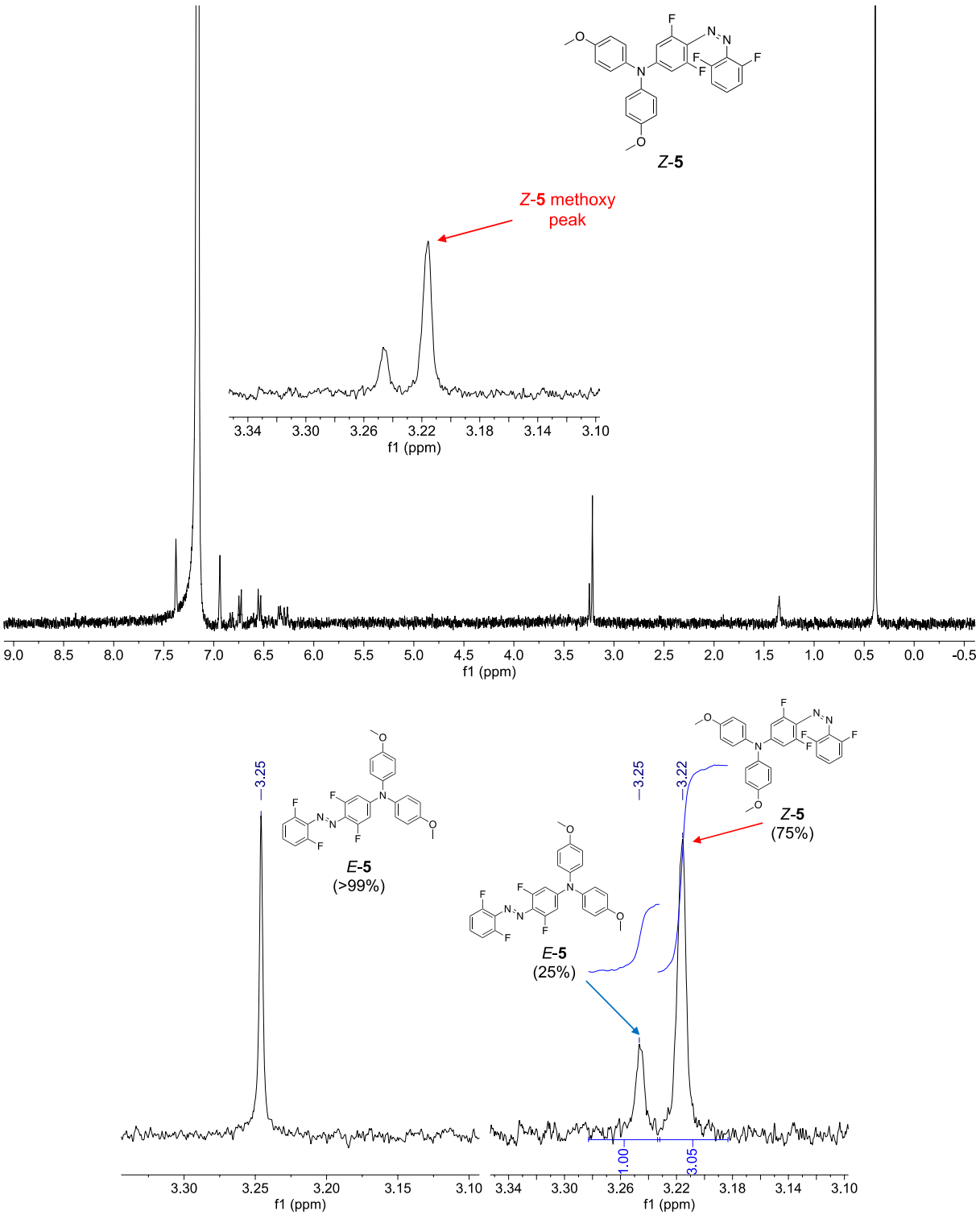

Figure S43. (top) Full spectrum view of the ^{1}H NMR spectrum (500 MHz) of the mixture of *E*-**5** and *Z*-**5** ([**5**] = 2.5 x 10^{-4} M in deaerated C_6D_6) at the 395-410 nm PSS. (bottom) Methoxy regions of the ^{1}H NMR spectra of 2.5 x 10^{-4} M *E*-**5** in deaerated C_6D_6 (left) and the mixture of *E*-**5** (25%) and *Z*-**5** (75%) at the PSS (right), which was reached by irradiating the sample with a 7 W 395-410 nm LED source.

5. *Z*→*E* thermal isomerization of 2-4 followed by UV-vis spectroscopy

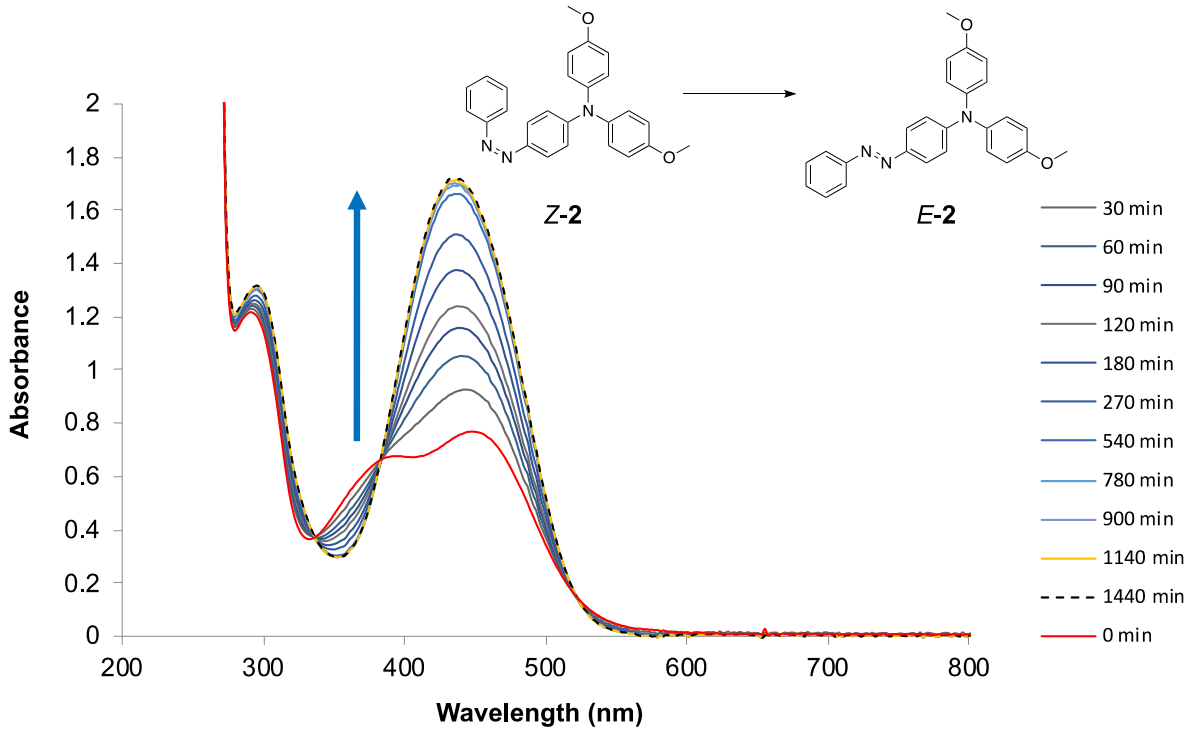

Figure S44. Overlay of optical spectra recorded at different times during the *Z*-**2**→*E*-**2** thermal isomerization process occurring in the dark at 295 K ([**2**] = 6.35 x 10^{-4} M in deaerated C_6D_6 in a 0.1 cm quartz cuvette).

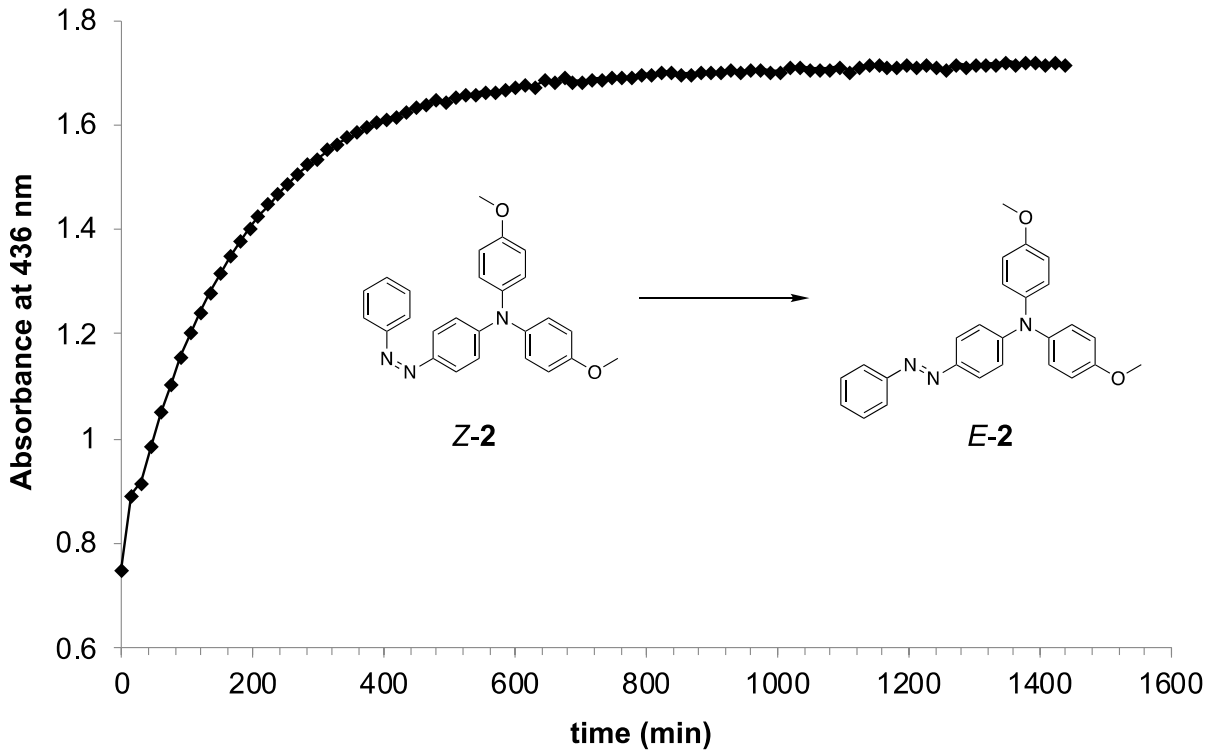

Figure S45. Time radiation profile following absorbance at 436 nm with respect to time during the *Z*-**2**→*E*-**2** thermal isomerization process occurring in the dark at 295 K ([**2**] = 6.35 x 10^{-4} M in deaerated C_6D_6 in a 0.1 cm quartz cuvette).

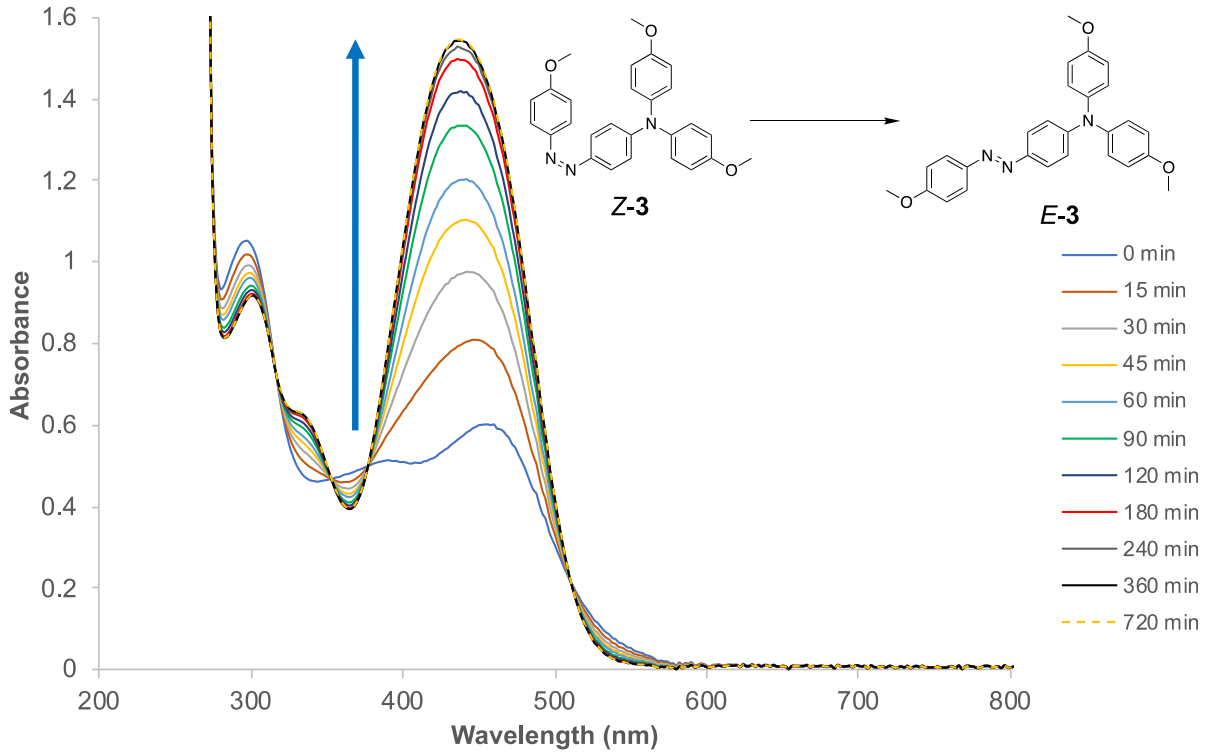

Figure S46. Overlay of optical spectra recorded at different times during the *Z*-**3**→*E*-**3** thermal isomerization process occurring in the dark at 295 K ([**3**] = 6.37 x 10^{-4} M in deaerated C_6D_6 in a 0.1 cm quartz cuvette).

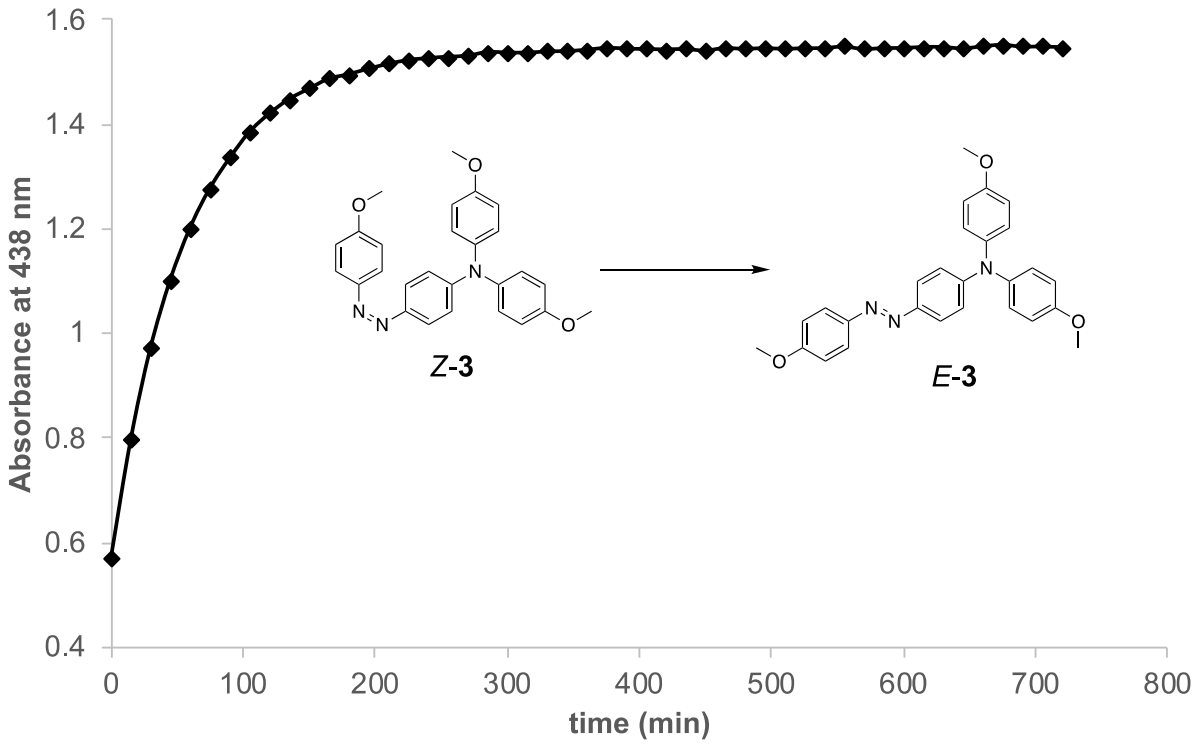

Figure S47. Time radiation profile following absorbance at 436 nm with respect to time during the *Z*-**3**→*E*-**3** thermal isomerization process occurring in the dark at 295 K ([**3**] = 6.37 x 10^{-4} M in deaerated C_6D_6 in a 0.1 cm quartz cuvette).

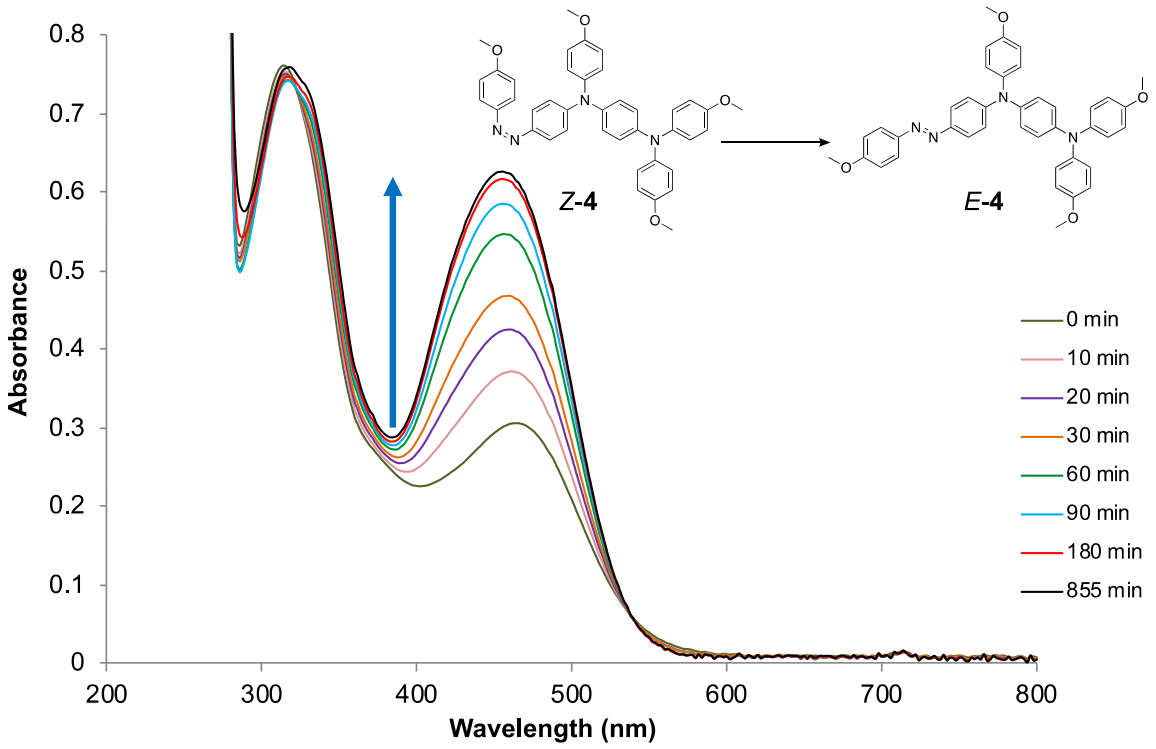

Figure S48. Overlay of optical spectra recorded at different times during the *Z*-**4**→*E*-**4** thermal isomerization process occurring in the dark at 295 K ([**4**] = 3.14 x 10^{-4} M in deaerated benzene in a 0.1 cm quartz cuvette).

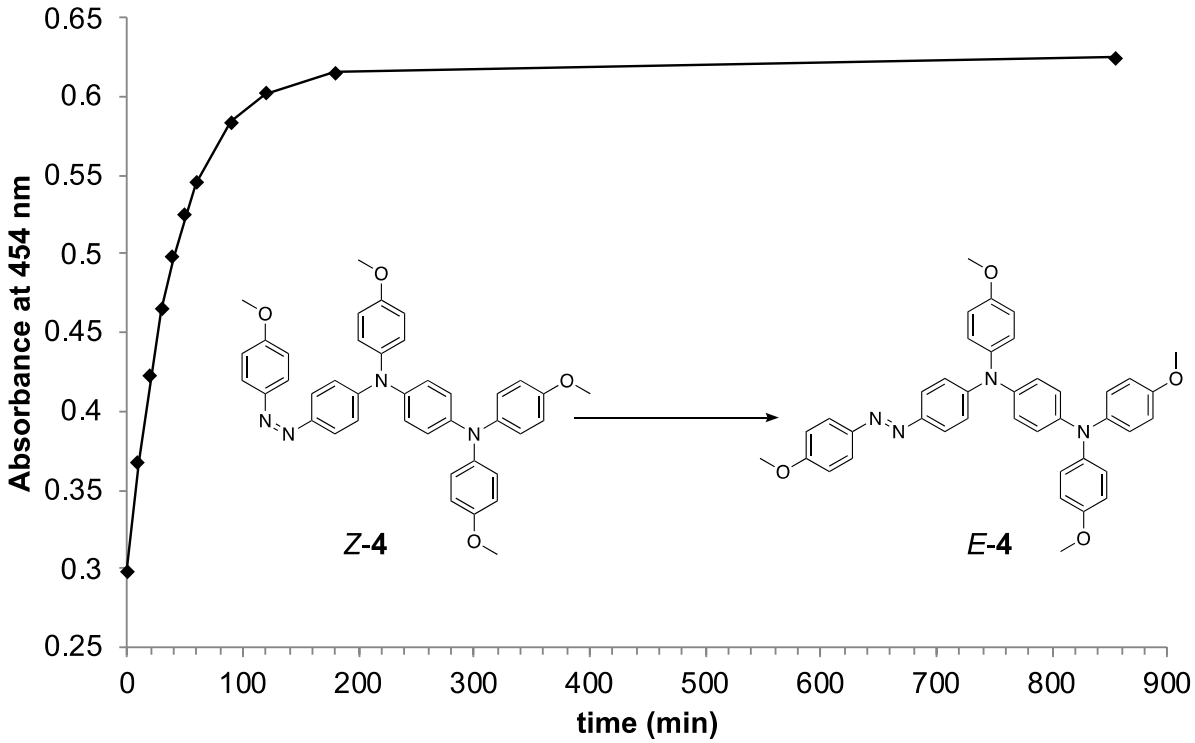

Figure S49. Time radiation profile following absorbance at 454 nm with respect to time during the *Z*-**4**→*E*-**4** thermal isomerization process occurring in the dark ([**4**] = 3.14 x 10^{-4} M in deaerated benzene).

6. ln[C] vs. time plots for 2-4 used to determine rate constants, half-lives and thermodynamic parameters for *Z*→*E* thermal isomerization

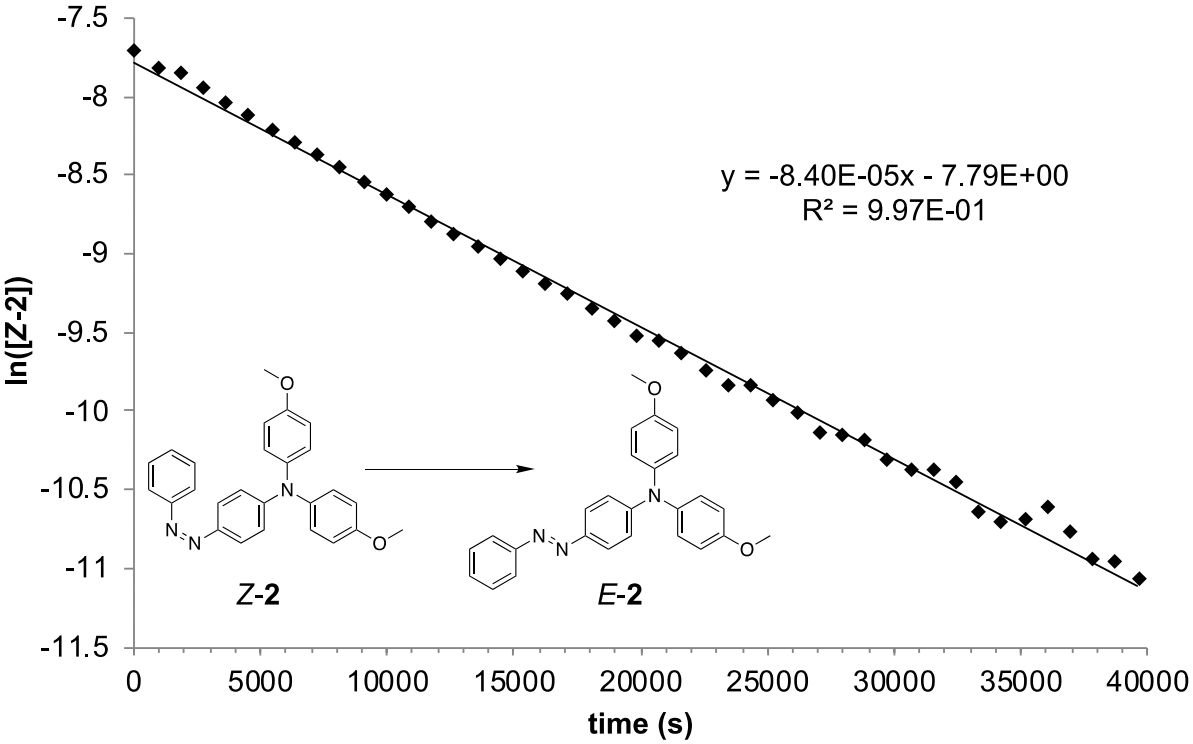

Figure S50. Plot of ln[*Z*-**2**] vs. time used to determine the rate constant (k = 8.40 ± 0.07 x 10^{-5} s^{-1}), half-life ($t_{1/2}$ = 2 h 18 min) and Gibbs free energy of activation ($\Delta G^{\ddagger}$ = 22.8 ± 0.1 kcal/mol) for the *Z*-**2**→*E*-**2** thermal isomerization process. ([**2**] = 6.35 x 10^{-4} M in deaerated C_6D_6 in a 0.1 cm cuvette at 295 K)

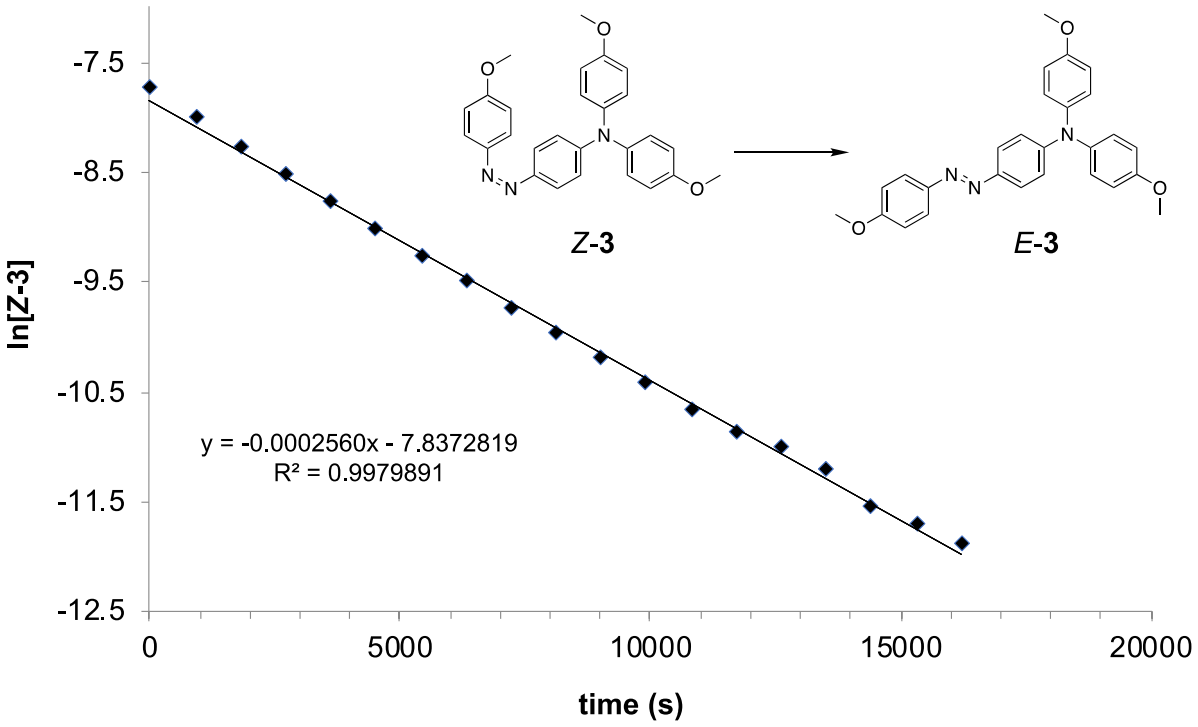

Figure S51. Plot of ln[*Z*-**3**] vs. time used to determine the rate constant (k = 2.88 ± 0.02 x 10^{-4} s^{-1}), half-life ($t_{1/2}$ = 40 min) and Gibbs free energy of activation ($\Delta G^{\ddagger}$ = 22.0 ± 0.1 kcal/mol) for the *Z*-**3**→*E*-**3** thermal isomerization process. ([3] = 6.37 x 10^{-4} M in deaerated C_6D_6 in a 0.1 cm cuvette at 295 K)

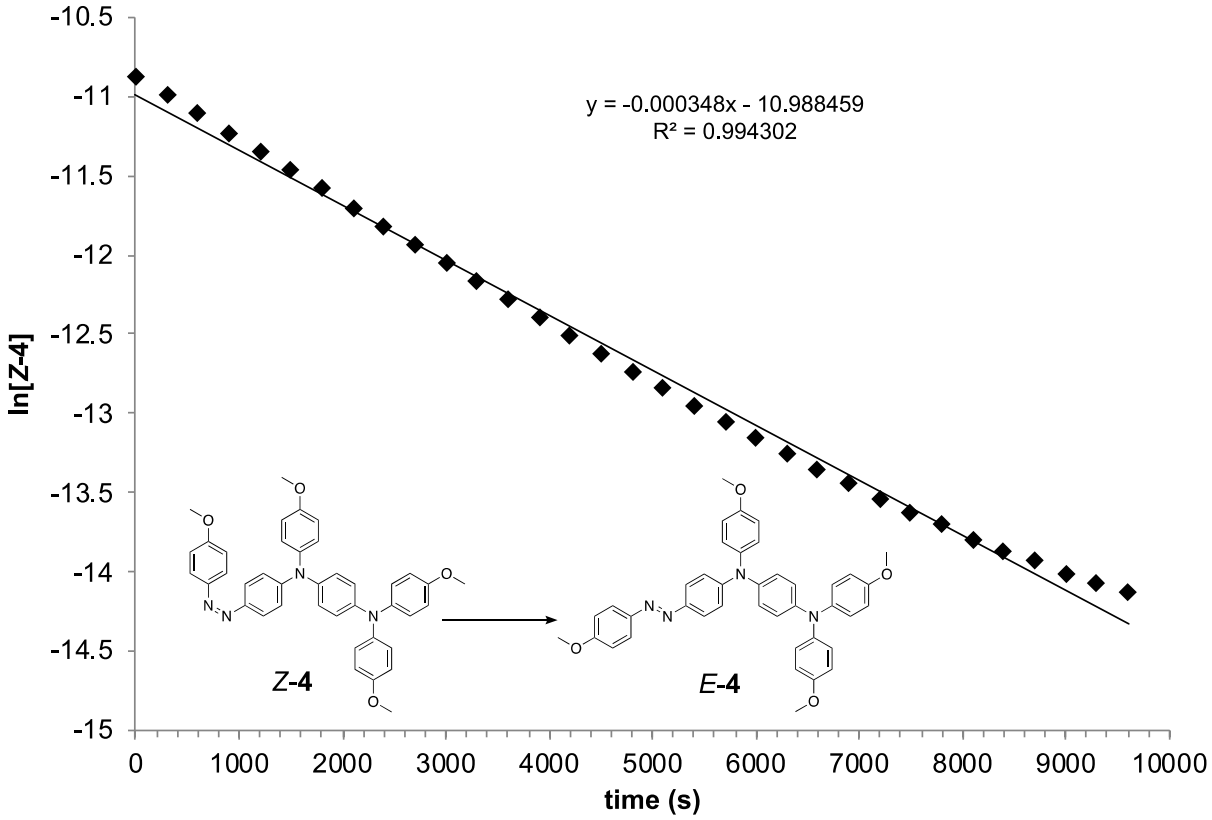

Figure S52. Plot of ln[*Z*-**4**] vs. time used to determine the rate constant (k = 3.48 ± 0.05 x 10^{-4} s^{-1}), half-life ($t_{1/2}$ = 33 min) and Gibbs free energy of activation ($\Delta G^{\ddagger}$ = 21.9 ± 0.1 kcal/mol) for the *Z*-**4**→*E*-**4** thermal isomerization process. ([**4**] = 3.14 x 10^{-4} M in deaerated benzene in a 0.1 cm cuvette at 295 K).

7. Equations and methodology for determination of the rate constant, half-life and Gibbs free energy of activation for the *Z*→*E* thermal isomerization process of a given monoazobenzene

The rate at which *Z* converts to *E* depends on the concentration of the reactants present in the solution. The rate can be represented by the following equation (**Eqn. 1**):

$$rate = k[Z] \qquad \textbf{(Eqn. 1)}$$

Given the UV-vis spectroscopic cell path length, *b*, the concentration of *E* isomer in the initial all *E* solution, $[E]_0$, and the absorbance, *A*, at the wavelength of maximum absorbance (λ_{max}), one can apply Beer's Law to determine the molar absorptivity coefficient for the *E* isomer at the wavelength of maximum absorbance, $\varepsilon_{\lambda_{max}(E)}$, as shown in **Eqn. 2**.

$$\varepsilon_{\lambda_{max}(E)} = \frac{A}{b \cdot [E]_0} \qquad \textbf{(Eqn. 2)}$$

The proportions of *Z* and *E* isomers, P_Z and P_E, respectively, at the photo stationary state (PSS) may be determined via ^{1}H NMR spectroscopy. The absorbance attributed to the *E* isomer at PSS, $A_{E@PSS}$, can be calculated using Beer's Law, as shown in **Eqn. 3**.

$$A_{E@\mathrm{PSS}} = \varepsilon_{\lambda_{max(E)}} \cdot b \cdot P_E \cdot [E]_0 \qquad \textbf{(Eqn. 3)}$$

So, given the total absorbance due to both the *Z* and *E* isomers at PSS, $A_{Z+E@PSS}$, and the absorbance attributed to the *E* isomer at PSS, the absorbance of *Z* at PSS, $A_{Z@PSS}$, can be obtained using **Eqn. 4**.

$$A_{Z@\mathrm{PSS}} = A_{E+Z@\mathrm{PSS}} - A_{E@\mathrm{PSS}} \qquad \textbf{(Eqn. 4)}$$

The molar absorptivity coefficient for the *Z* isomer at λ_{max}, $\varepsilon_{\lambda_{max(Z)}}$, can be found using the rearranged form of Beer's Law shown in **Eqn. 5**.

$$\varepsilon_{\lambda_{max(Z)}} = \frac{A_{Z@\mathrm{PSS}}}{b \cdot P_Z \cdot [E]_0} \qquad \textbf{(Eqn. 5)}$$

Now that ε_E and ε_Z have been determined for a given wavelength (in this example λ_{max}), we have the values required to calculate [*E*] or [*Z*] for any time *t*. One can write an expression for [*E*] as a function of *t* and then calculate [*Z*] for any time *t* using (**Eqn. 6**)

$$[total] = [E]_0 = [Z] + [E] \qquad (\textbf{Eqn. 6})$$

where $[E]_0$ is the initial concentration of *E* isomer prior to irradiation such that ~100% is in the *E* conformation. Rearranging to solve for [*Z*] gives **Eqn. 7**

$$[Z] = [E]_0 - [E] \qquad (\textbf{Eqn. 7})$$

However, one can bypass this step by solving directly for [*Z*] as a function of absorbance *A*, which depends on the amount of time passed after reaching the PSS.

The following steps show how to arrive at an expression for [*Z*]:

For A_{total}, the measured absorbance of the solution at a given time *t* after reaching the PSS, $A_{total} = A_Z + A_E$, where A_Z and A_E are the values for absorbance ascribed to the *Z* and *E* isomers, respectively, for a given time *t*.

Using Beer's law, we know that for a given wavelength (it is convenient to choose λ_{max} because this is the wavelength for which we already determined the extinction coefficients for *Z* and *E*),

$$A_Z = \varepsilon_Z \cdot b \cdot [Z] \qquad (\textbf{Eqn. 8})$$

and

$$A_E = \varepsilon_E \cdot b \cdot [E] \qquad (\textbf{Eqn. 9})$$

Thus, $A_{total} = A_E + A_Z = \varepsilon_E \bullet b \bullet [E] + \varepsilon_Z \bullet b \bullet [Z]$

At this point our equation contains one directly observable variable, A_{total}, and two variables that are not directly observable: [*Z*] and [*E*]. Above we specified in (**Eqn. 6**) that

$$[total] = [E]_0 = [Z] + [E] \quad \textbf{(Eqn. 6)}$$

This can be rearranged to solve for [*E*]:

$$[E] = [E]_0 - [Z] \quad \textbf{(Eqn. 10)}$$

Eqn. 10 can be substituted into the expression for A_{total} to eliminate [*E*] from the equation and obtain the following:

$$A_{total} = \varepsilon_E \cdot b \cdot ([E]_0 - [Z]) + \varepsilon_Z \cdot b \cdot [Z] \quad \textbf{(Eqn. 11)}$$

By grouping like terms, this can be rearranged to the following:

$$A_{total} = \varepsilon_E \cdot b \cdot [E]_0 + ([\varepsilon]_Z \cdot b - [\varepsilon]_E \cdot b) \cdot [Z] \quad \textbf{(Eqn. 12)}$$

Lastly, solving for [*Z*] gives:

$$[Z] = \frac{A_{total} - \varepsilon_E \cdot b \cdot [E]_0}{\varepsilon_Z \cdot b - \varepsilon_E \cdot b} \quad \textbf{(Eqn. 13)}$$

Given that $A_0 = \varepsilon_E \bullet b \bullet [E]_0$, where A_0 is the absorbance prior to irradiation such that only the *E* isomer is present, we can simplify the above expression to obtain **Eqn. 14**

$$[Z] = \frac{A_{total} - A_0}{\varepsilon_Z \cdot b - \varepsilon_E \cdot b} \quad \textbf{(Eqn. 14)}$$

With this expression one can determine [*Z*] for various times throughout the thermal isomerization process based on the values for absorbance recorded at those times, which allows for the calculation of ln[*Z*] for all such times. Plotting ln[*Z*] vs. time gives a line having a slope (*m*) equal to the negative of the rate constant, *k* (*m* = -*k*).

The half-life, $t_{1/2}$, for the *Z*→*E* thermal isomerization process is determined using the relation

$$t_{1/2} = \ln(2)/k \quad \textbf{(Eqn. 15)}$$

One can also calculate Gibbs free energy of activation, $\Delta G^{\neq}$, using the Eyring equation. The equation expressed in its exponential form is shown below:

$$k = \kappa \left(\frac{k_B T}{h}\right) e^{(-\Delta G^{\neq}/RT)} \quad \textbf{(Eqn. 16)}$$

where k_B is the Boltzmann constant (1.38 x 10^{-23} J/K), *T* is temperature (in units of Kelvin), *h* is the Planck constant (6.63 x 10^{-34} J•S), *R* is the ideal gas constant (8.314 J/mol•K) and κ is a

factor known as the transmission coefficient. (The transmission coefficient takes into account that not every vibrational oscillation will convert the activated complex (i.e. the excited state in our case) to the product. However, for monomolecular processes κ is usually assumed to equal 1.) Assuming $\kappa = 1$ and taking the natural logarithm of both sides gives

$$\ln(k) = ln\left(\frac{k_B T}{h}\right) - \frac{\Delta G^{\neq}}{RT} \quad \textbf{(Eqn. 17)}$$

Solving for $\Delta G^{\neq}$ gives

$$\Delta G^{\neq} = RT\left[ln\left(\frac{k_B T}{h}\right) - \ln(k)\right] \quad \textbf{(Eqn. 18)}$$

Thus, the rate constant *k* can be used to solve for the Gibbs free energy of activation, $\Delta G^{\neq}$, for the *Z*→*E* thermal isomerization process for a given azobenzene.

8. ln[C] vs. time plots used to determine *Z*→*E* thermal rate constants for 5 at multiple temperatures

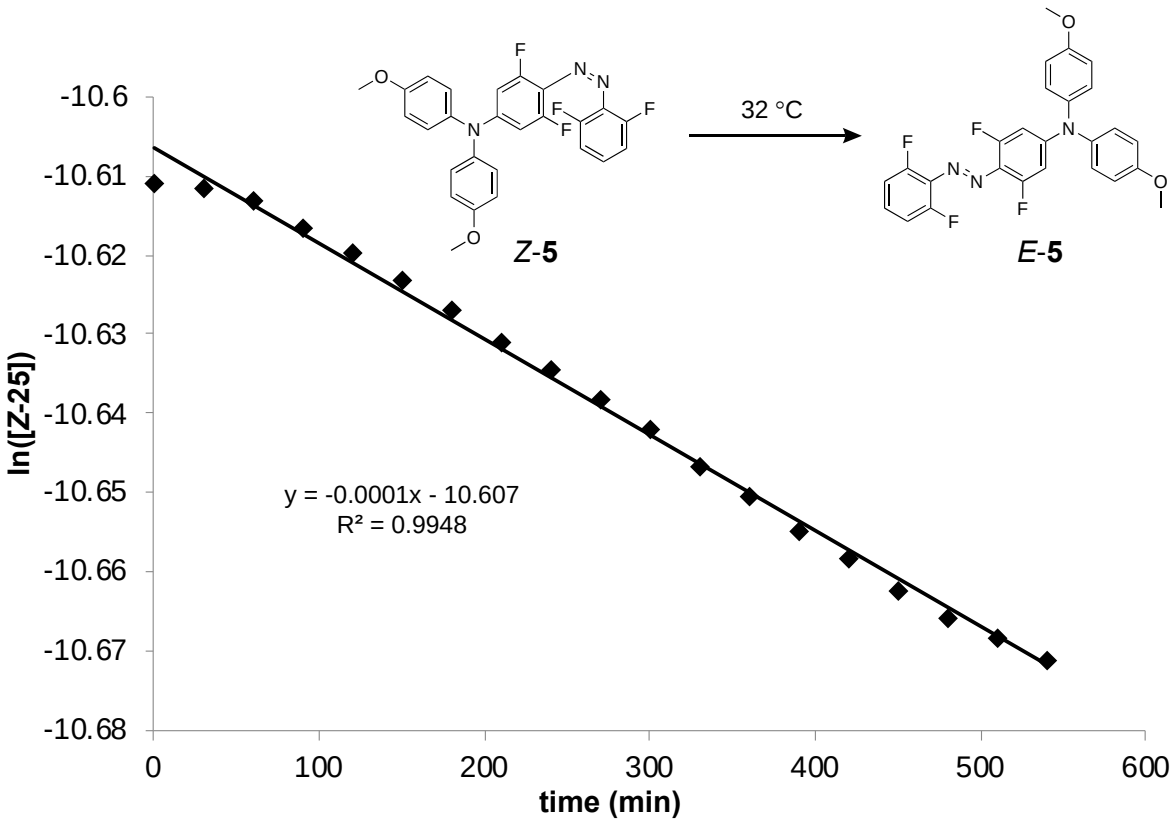

Figure S53. Plot of ln[*Z*-**5**] vs. time used to determine the rate constant ($k_{305\ K}$ = 2.02 ± 0.04 x 10^{-6} s^{-1}) for the *Z*-**5**→*E*-**5** thermal isomerization process at 32 °C. UV-vis spectroscopic measurements were recorded in the dark. ([**5**] = 3.5 x 10^{-5} M in deaerated C_6D_6 in a 1.0 cm quartz cuvette at 305 K)

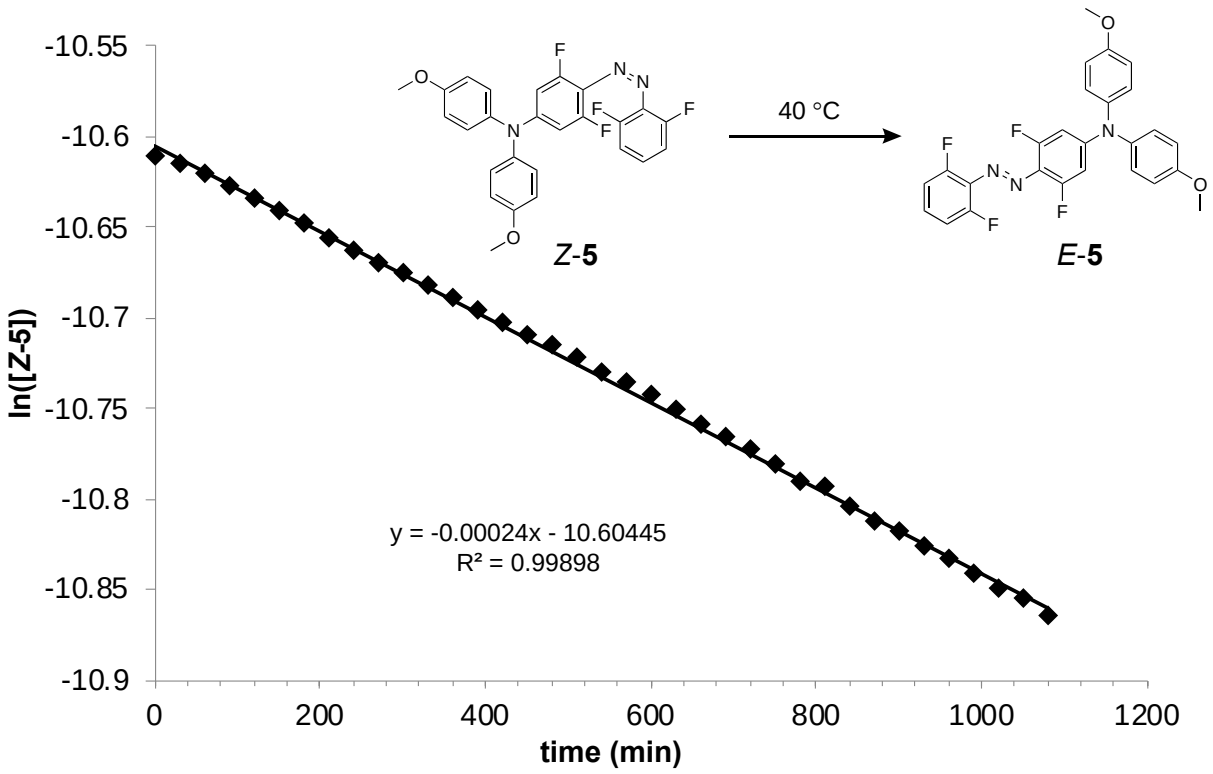

Figure S54. Plot of ln[*Z*-**5**] vs. time used to determine the rate constant ($k_{313\,K}$ = 3.93 ± 0.02 x 10^{-6} s^{-1}) for the *Z*-**5**→*E*-**5** thermal isomerization process at 40 °C. UV-vis spectroscopic measurements were recorded in the dark. ([**5**] = 3.5 x 10^{-5} M in deaerated C_6D_6 in a 1.0 cm quartz cuvette at 313 K)

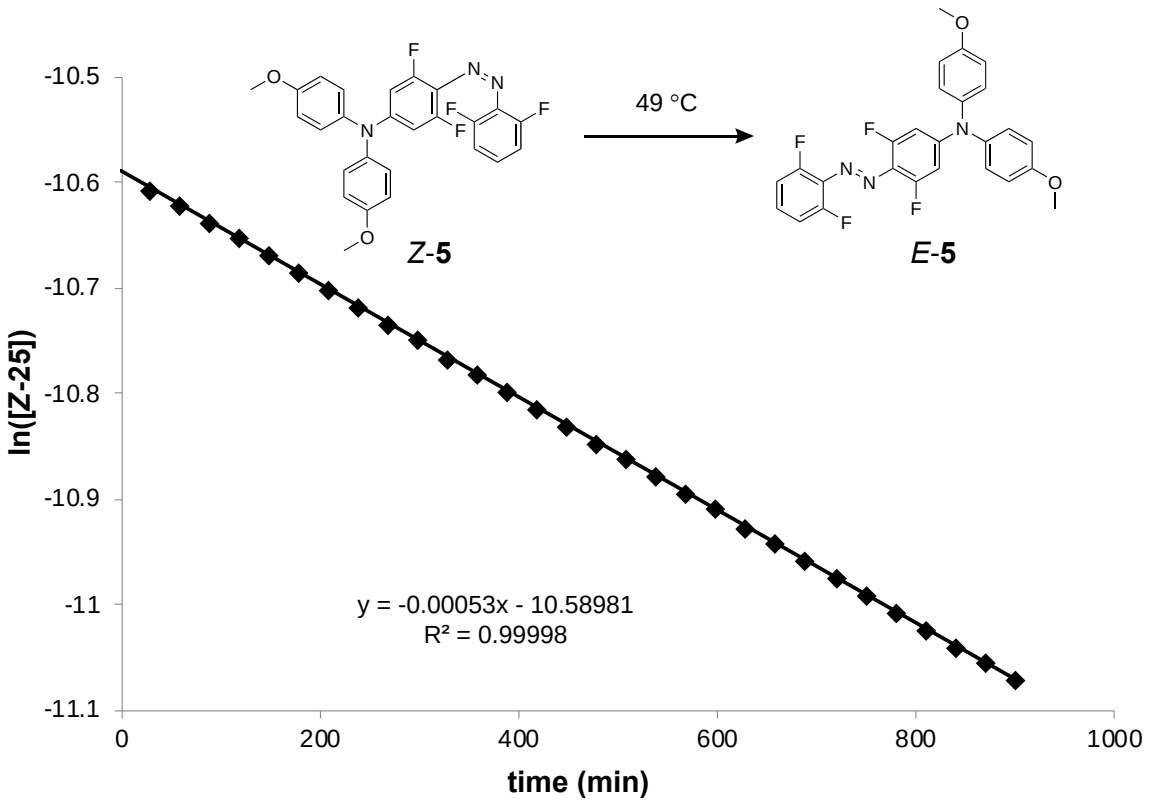

Figure S55. Plot of ln[*Z*-**5**] vs. time used to determine the rate constant ($k_{322\ K}$ = 8.83 ± 0.04 x 10^{-6} s^{-1}) for the *Z*-**5**→*E*-**5** thermal isomerization process at 49 °C. UV-vis spectroscopic measurements were recorded in the dark. ([**5**] = 3.5 x 10^{-5} M in deaerated C_6D_6 in a 1.0 cm quartz cuvette at 322 K)

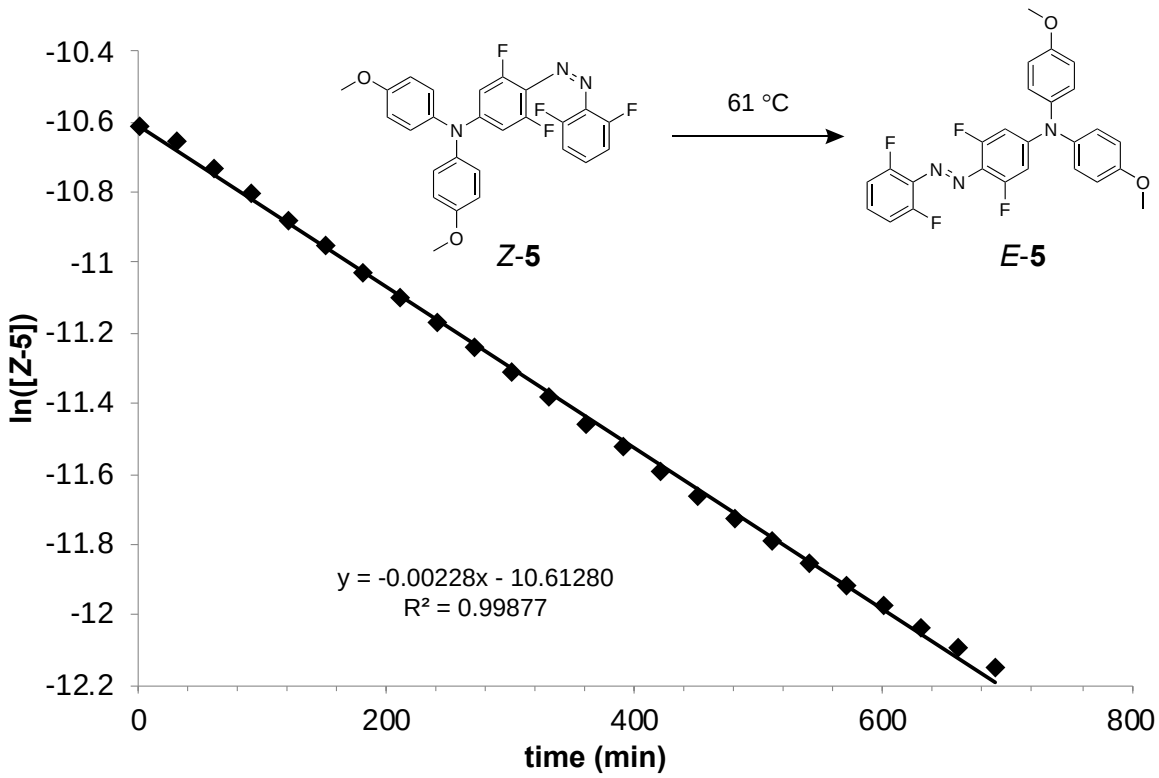

Figure S56. Plot of ln[*Z*-**5**] vs. time used to determine the rate constant ($k_{334\,K}$ = 3.80 ± 0.03 x 10^{-5} s^{-1}) for the *Z*-**5**→*E*-**5** thermal isomerization process at 61 °C. UV-vis spectroscopic measurements were recorded in the dark. ([**5**] = 3.5 x 10^{-5} M in deaerated C_6D_6 in a 1.0 cm quartz cuvette at 334 K)

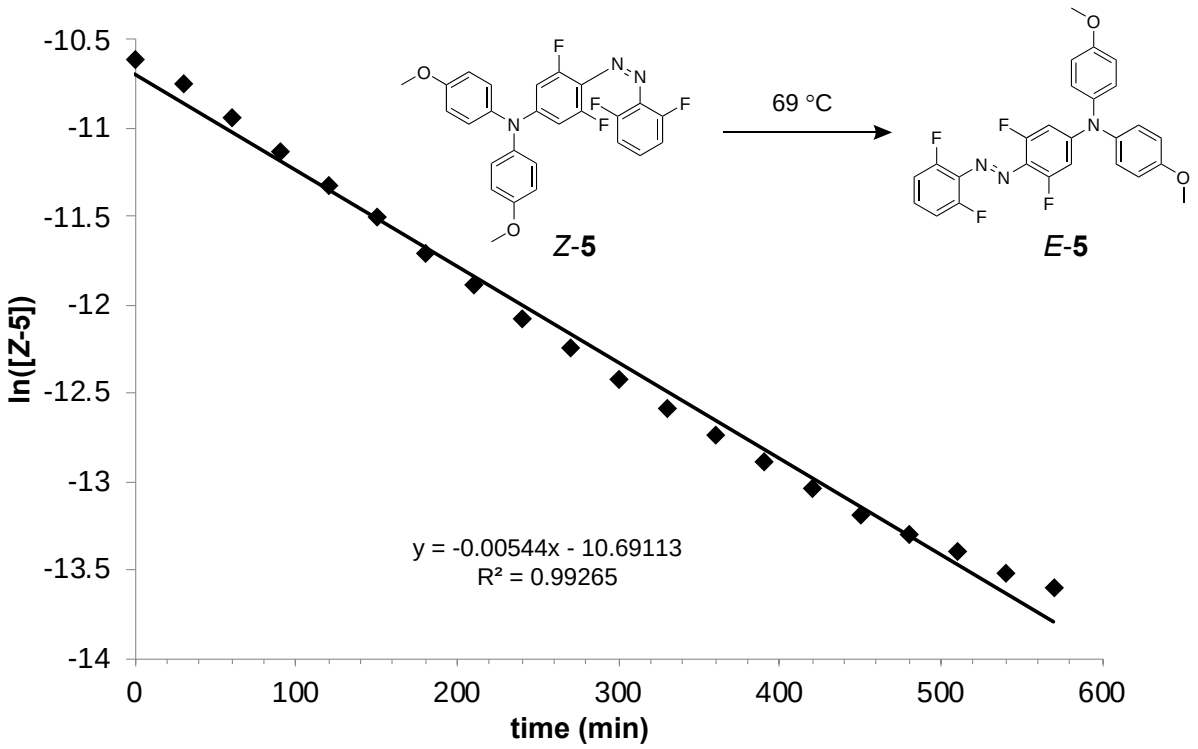

Figure S57. Plot of ln[*Z*-**5**] vs. time used to determine the rate constant ($k_{342\ K}$ = 9.07 ± 0.18 x 10^{-5} s^{-1}) for the *Z*-**5**→*E*-**5** thermal isomerization process at 69 °C. UV-vis spectroscopic measurements were recorded in the dark. ([**5**] = 3.5 x 10^{-5} M in deaerated C_6D_6 in a 1.0 cm quartz cuvette at 342 K)

9. Eyring plot for *Z*-5→*E*-5 thermal conversion used to extract the enthalpy and entropy of activation, from which the rate constant, half-life and Gibbs free energy of activation for the process at room temperature may be extrapolated

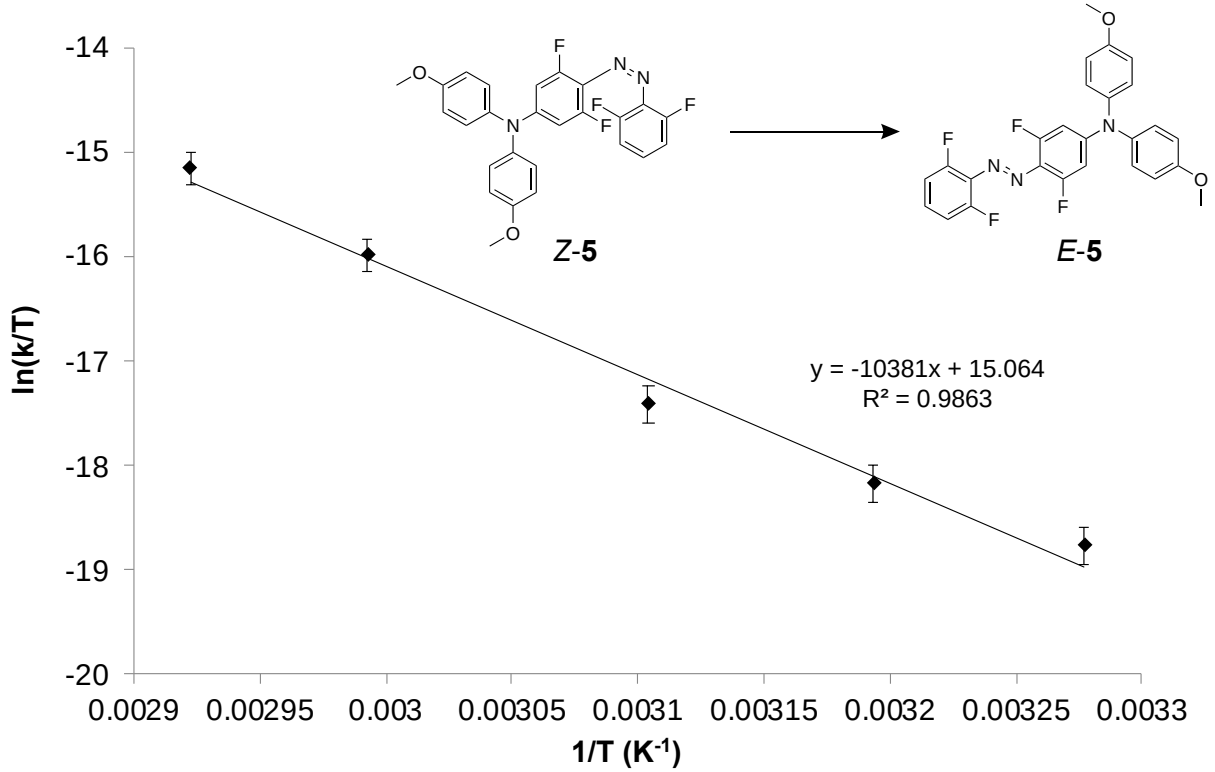

Figure S58. Eyring plot of ln(*k*/*T*) vs. 1/*T* for [**5**] = 3.5 x 10^{-5} M in deaerated C_6D_6, where *k* is the rate constant for *Z*→*E* thermal isomerization at a given absolute temperature, *T*, in Kelvins. UV-vis spectroscopic measurements were taken in the dark in a 1.0 cm quartz cuvette, for which the temperature was controlled using a heated cuvette holder. The enthalpy of activation ($\Delta H^{\ddagger}$ = 20.6 kcal/mol ± 1.4 kcal/mol) and entropy of activation ($\Delta S^{\ddagger}$ = -17.3 eu ± 4.4 eu) were determined from this plot. Using these values in conjunction with the equation $\Delta G^{\ddagger} = \Delta H^{\ddagger} - T\Delta S^{\ddagger}$, the rate constant ($k_{295\ K}$ = 5.58 ± 18.1 x 10^{-7} s^{-1}), Gibbs free energy of activation ($\Delta G^{\ddagger}$ = 25.7 kcal/mol ± 1.9 kcal/mol) and the half-life ($t_{1/2}$ = 14 days) for this process at 295 K were extrapolated.

10. UV-vis spectra following ET catalytic *Z*→*E* switching of 3-5

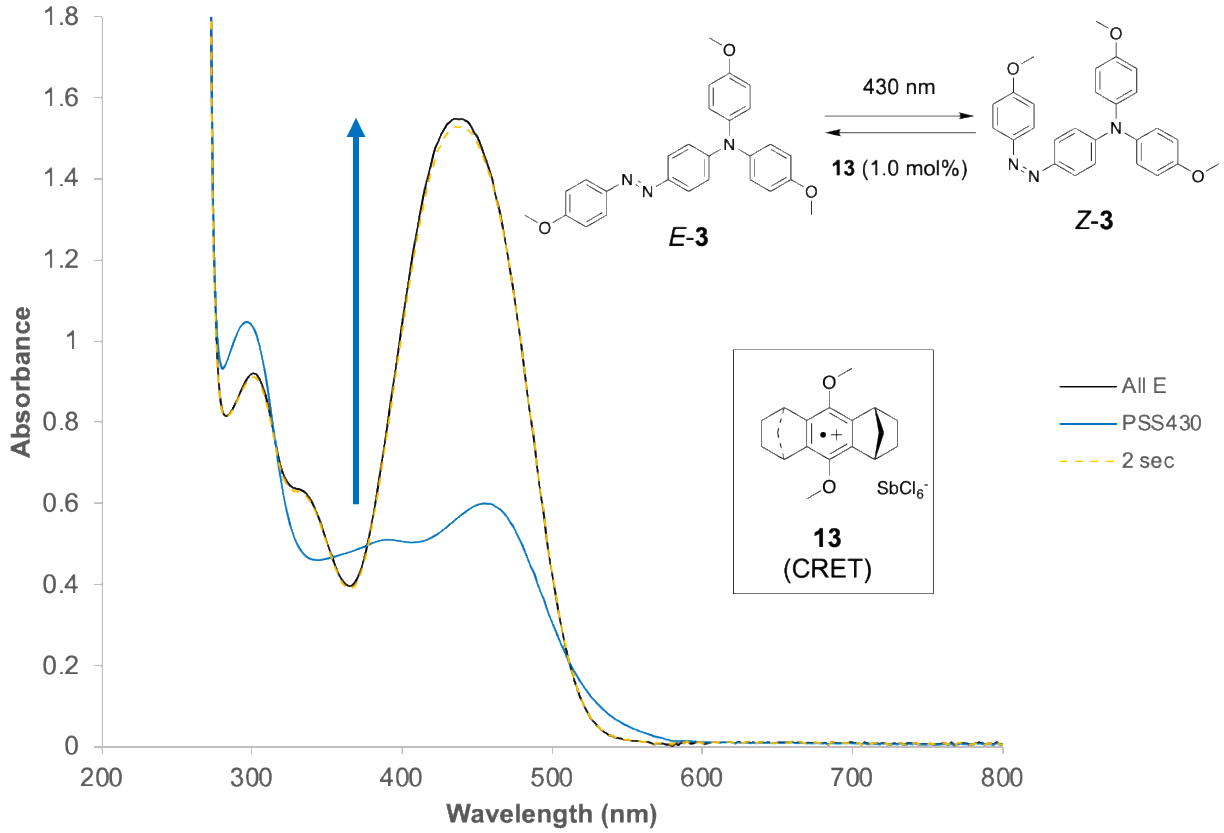

Figure S59. Overlay of optical spectra of **3** (6.37 x 10^{-4} M in C_6D_6 in a 0.1 cm quartz cuvette) taken prior to irradiation, after irradiation at the 430 nm PSS and after addition of 1.0 mol% oxidant **13** and shaking for 2 s. Absorbance from 200 nm to 800 nm was recorded every second.

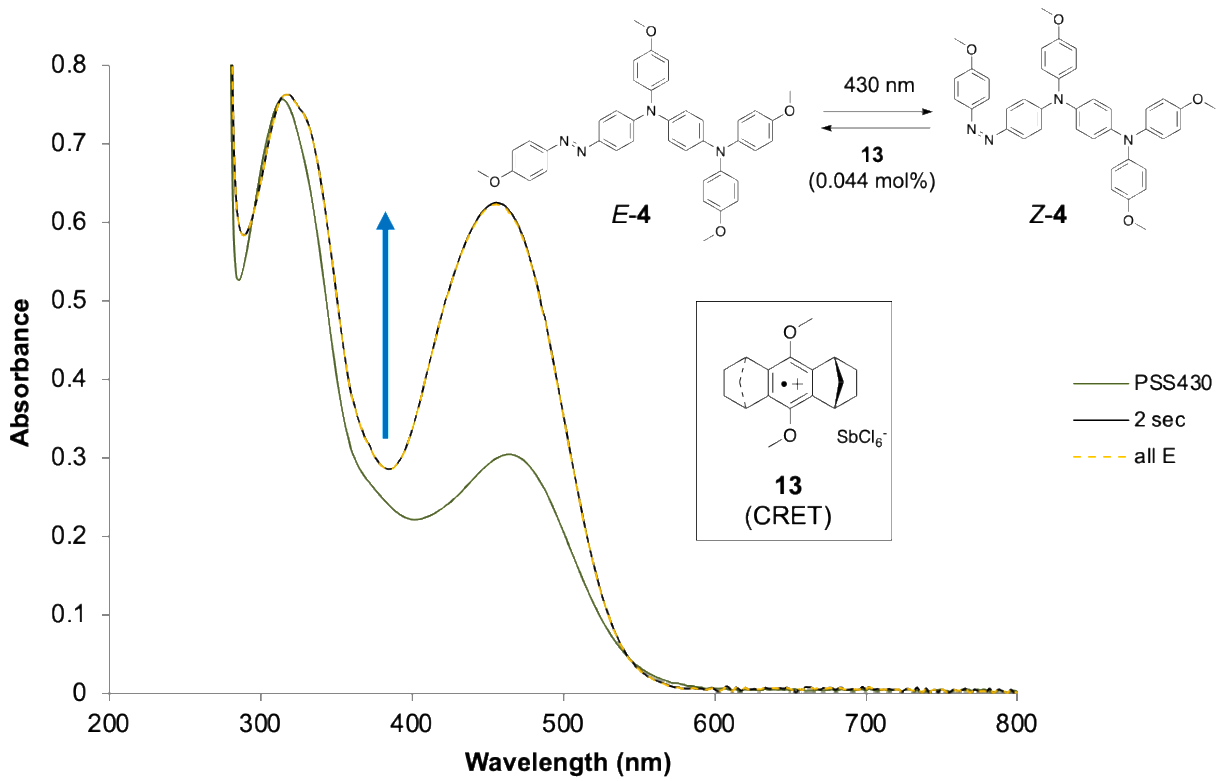

Figure S60. Overlay of optical spectra of **4** (3.1 x 10^{-5} M in benzene in a 1.0 cm quartz cuvette) taken prior to irradiation, after irradiating to the 430 nm PSS and after addition of 0.044 mol% oxidant **13** and shaking for 2 s. Absorbance from 200 nm to 800 nm was recorded every second. T = 295 K

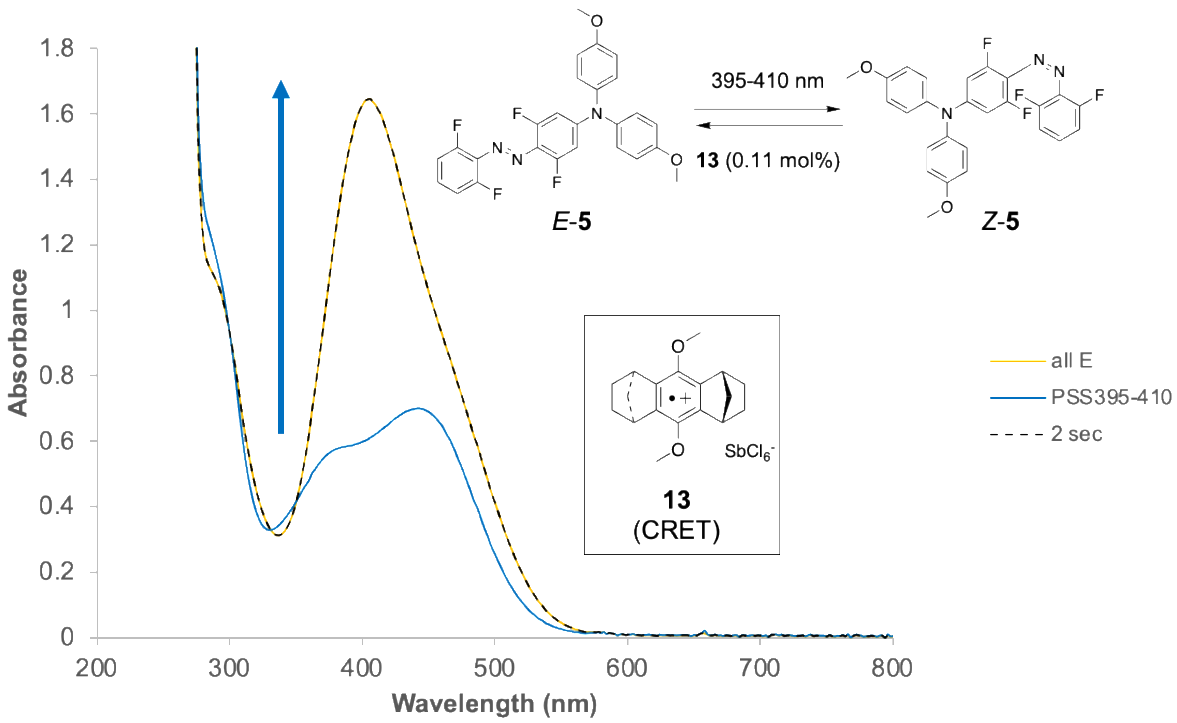

Figure S61. Overlay of optical spectra of **5** (5.5 x 10^{-4} M in benzene in a 0.1 cm quartz cuvette) taken prior to irradiation, after irradiating to the 395-410 nm PSS and after addition of 0.11 mol% oxidant **13** and shaking for 2 s. Absorbance from 200 nm to 800 nm was recorded every second.

11. EPR Spectra of $3^{\bullet+}PF_6^-$ and $4^{\bullet+}PF_6^-$ Radical Cation Salts

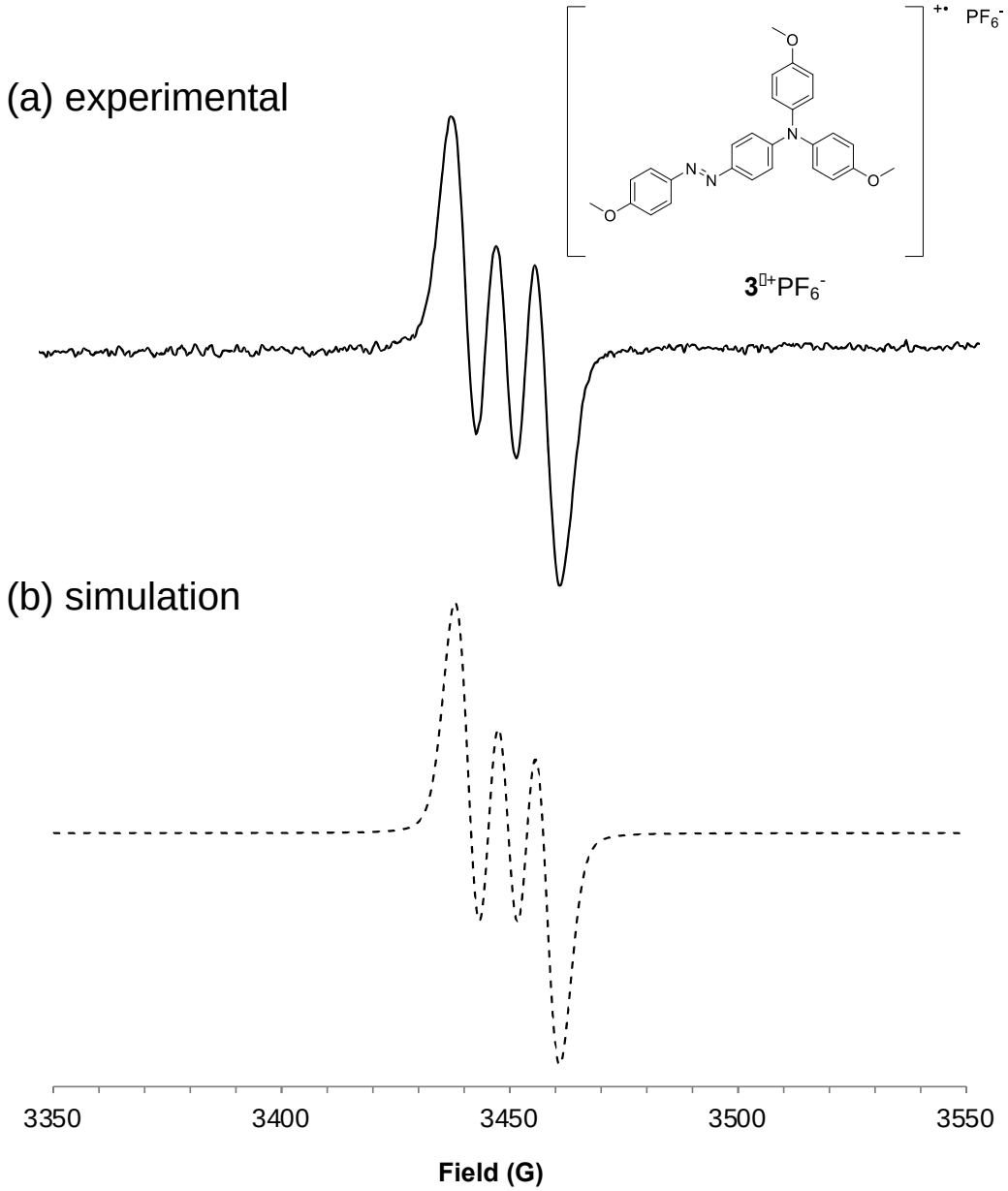

Figure S62. (a) CW EPR spectrum of $\mathbf{3}^{\bullet+}PF_6^-$ (2.0 mM) in purified and distilled DCM taken at 293 K on a ELEXSYS E680 EPR spectrometer (Bruker-Biospin, Billerica, MA) equipped with a Bruker Flexline ER 4118 CF cryostat and an ER 4118X-MD4 ENDOR resonator. (b) Simulation spectrum parameters are 5.64, 1.31 G (Gaussian, Lorentzian contribution) line width and a(N) ≈ 8.2 G.

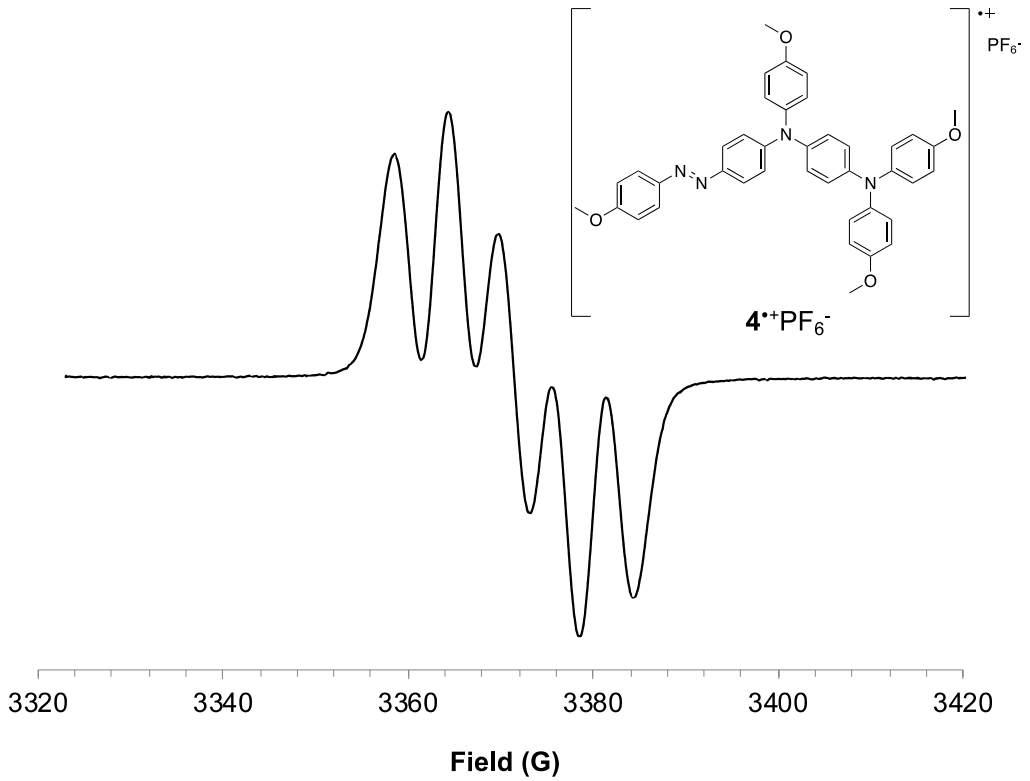

Figure S63. CW EPR spectrum of **4**$^{\bullet+}PF_6^-$ (1.00 mM) in DCM taken on a Bruker ER082 x-band spectrometer at 298 K, a(2N) ≈ 5.7 G.